Supramolecular Side-Chain Liquid Crystalline Polymers with Various Kinked Pendant Groups

Hong-Cheu Lin,* Yen-Shyi Lin, Yu-Sheng Lin, Yao-Te Chen, Ito Chao, and Ta-Wei Li

Institute of Chemistry, Academia Sinica, Taipei, Taiwan, Republic of China

Received May 7, 1998; Revised Manuscript Received August 10, 1998

ABSTRACT: Supramolecular side-chain liquid crystalline polymers with various kinked pendant groups are constructed from positional isomers of proton acceptor monomers and donor polymers (with different molecular weights) through hydrogen bonding. Monomer−monomer complexes of similar structures are built to compare the influence of the proton donors bound to the polymer backbones. Due to the bending effects introduced by the positional isomers, we are able to tune the molecular shape and thus to modify the mesogenic properties. New liquid crystalline properties are introduced by the kinked molecular geometry, and their kinked architecture is supported by the quantum mechanical calculations, the powder X-ray diffraction (XRD) patterns, and the deviation temperatures (ΔT). Mesogenic properties of monomer−polymer complexes have similar trends as those of monomer−monomer complexes. Compared with analogous hydrogen-bonded (H-bonded) monomer−monomer complexes, higher isotropization temperatures and broader ranges of mesogenic phases (e.g., S_A phase) are observed in the kinked supramolecular polymers. Significantly, H-bonded positional isomerism leads to dissimilar structures and properties of supramolecular side-chain liquid crystalline polymers.

Introduction

Recently, self-assembled phenomena through the molecular recognition between individual constituents have been explored in various areas.[1−4] Hydrogen bonding is one of the most important key factors for the molecular recognition in nature. Intensive investigation has been concentrated on the usage of noncovalent interactions, such as ionic force[5,6] and hydrogen bonding,[7−16] to generate liquid crystalline polymers. Lehn and co-workers have demonstrated supramolecular liquid crystals using multiple hydrogen bonds to form a main-chain polymeric supramolecular rigid rod.[7] In another aspect, side-chain liquid crystalline polymers have great potential in various utilization as novel technological materials, such as optical switching elements, optical storage devices, and information displays. Normally, side-chain liquid crystalline polymers consist of polymer backbones, flexible spacers, and mesogenic pendant groups. Most of the mesogens are covalently attached to the polymer backbones through the flexible spacers. The function of the spacers is to decoupling the motion of the polymer backbones from the self-ordering of the mesogens. Nevertheless, instead of linking pendant groups covalently to the side chains of the polymers, novel mesogenic properties can also be easily obtained through the noncovalent linkage (i.e., hydrogen bond), and thus the hydrogen-bonded side-chain liquid crystalline polymers are of special interest to several research laboratories.[7−21] Among their approaches, intermolecular hydrogen bonding is easily obtained by complexation of carboxylic (or benzoic) acid and pyridyl moieties. Several series of H-bonded complexes and side-chain liquid crystalline polymers through intermolecular hydrogen bonding (between benzoic acid and pyridyl interactions) have been reported lately.[10−14]

There are a few types of supramolecular side-chain liquid crystalline polymers (monomer−polymer complexes) that contain hydrogen bonds located near the polymer backbones or near the end of the spacers (or even embodied in the pendant mesogens). Supramolecular side-chain liquid crystalline polymers (monomer−polymer complexes) may contain both or either (or even neither) constituents (polymers and pendant monomers) possessing liquid crystallinity; however, the liquid crystallinity can be generated or can be altered through hydrogen bonding. Supramolecular side-chain polymers that contain hydrogen bonds located near the polymer backbones of the side-chain polymers have been reported recently.[17−21] To prove the existence of this kind of supramolecular side-chain polymer, different proton donors, i.e., acids (**1**−**3**), were complexed not only with

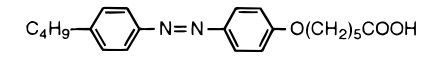

1

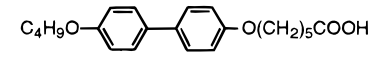

2

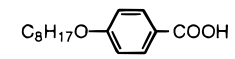

3

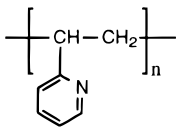

P2VP

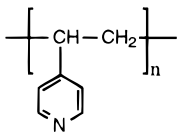

P4VP

poly(4-vinylpyridine) (P4VP) but also with poly(2-vinylpyridine) (P2VP) (or with polystyrene).[17−22] However, similar thermal behavior of these complexes, which contain either P4VP or P2VP with acids (**1**−**3**), suggested that limited miscibility of the proton acceptors and the acids has occurred. Few supramolecular side-chain polymers have formed in these types of complexes, though various degrees of hydrogen bonding between poly(vinylpyridines) (P4VP or P2VP) and proton donors

10.1021/ma980720e CCC: $15.00 © 1998 American Chemical Society
Published on Web 09/30/1998

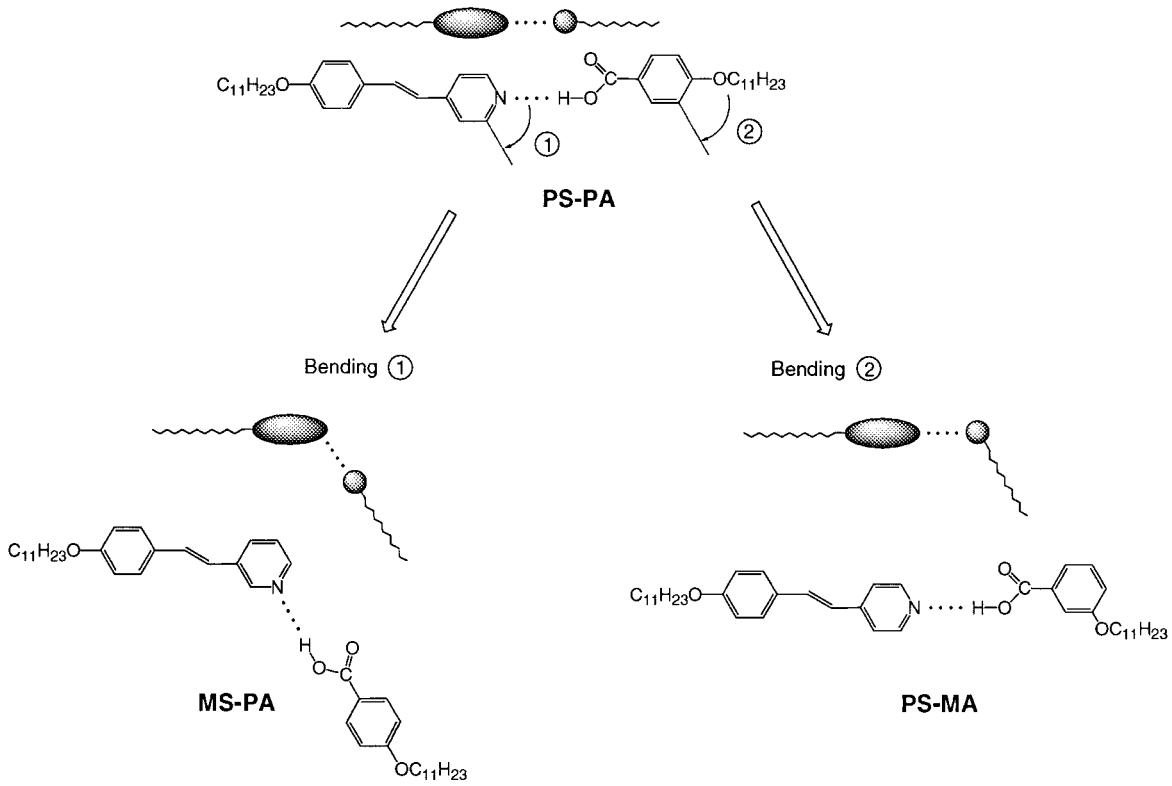

Figure 1. Kinked hydrogen-bonded complexes (monomer−monomer) bending at different sites.

(acids or alcohols) were reported in the literature.[23−26] It was also demonstrated that in order to construct the supramolecular side-chain liquid crystalline polymers by connecting the monomers to the polymer backbones noncovalently, the strength of the hydrogen bond should be large by using complementary units containing multiple binding sites to prevent proton transfer. Hence, these different isomeric complexes containing P4VP or P2VP could not be distinguished due to the phase separation, and the molecular mixing only occurred at relatively low concentrations of the proton donors.[19] Lately, many efforts have been made to synthesize proton acceptors copolymerized with mesogenic units in order to increase the miscibility of the proton donors in the complexes.[22] However, as expected, the supramolecular side-chain copolymers containing P2VP reveal worse mesogenic properties than those containing P4VP due to the steric hindrance of P2VP in the supramolecular side-chain polymers. Therefore, the pyridyl groups in P2VP polymers only offer poor (stericly hindered) hydrogen bonding sites as proton acceptors in the supramolecular complexes, and it is difficult to illustrate the pronounced effects of binding angles, i.e., positional isomerism, on supramolecular side-chain polymers involving P2VP or P4VP as proton acceptors.

Here, we would like to report the results acquired by complexation of the functional polymers and small molecules to form monomer−polymer complexes bearing hydrogen bonds, which are far away from the polymer backbones and are part of the mesogens in our study. The benzoic acid is separated from the main chain (ploysiloxane) by the alkoxyl spacer as a pendant group of the side chain of the polymer. The proton donor polymers are complexed with proton acceptors (i.e., stilbazoles and their derivatives). As we know, the kinked structures in mesogenic materials will lower the phase transition temperatures and will also mostly reduce the thermal stability of the liquid crystalline phases. Main-chain liquid crystalline polymers (LCPs) have successfully utilized this concept to reduce the processing temperature of the rigid architecture by the kinked and branched structures[27−29] in the application of LCPs. However, the effects of the nonlinear structures on the mesomorphism of side-chain liquid crystalline polymers, especially the H-bonded structures, remain unexplored so far. Only a few nonlinear H-bonded complexes (monomer−monomer) have been reported in the literature.[30−34] Therefore, we also would like to investigate the dependence of the mesomorphic properties on the supramolecular liquid crystalline polymers with kinked H-bonded side chains.

Our recent work has shown that different bending structures of various bending sites organized by the kinked H-bonded complexes (monomer−monomer) could reveal novel mesomorphic behavior.[33] To understand the effects of nonlinear geometry on both H-bonded complexes and supramolecular side-chain liquid crystalline polymers, the kinked structures are derived either from the kink between the rigid core and the flexible part or from the nonlinear rigid core bearing the kinked H-bond (Figure 1). Supramolecules (monomer−monomer complexes, i.e., PS−PA, PS−MA, MS−PA, PSO−PA, PSO−MA, and MSO−PA) with possible arrangements of various nonlinearities (bending positions of 1 and 2 in Figure 1), assuming a linear hydrogen bond between N···H−O (or O···H−O), were prepared from a 1:1 molar ratio of H-bonded acceptor[35,36] and donor moieties. Most importantly, we would like to report the mesogenic properties of the first supramolecular side-chain polymers containing various kinked pendant groups in this manuscript. These H-bonded donor polymers consist of polysiloxanes possessing different pendant *p*- (or *m*-) alkoxybenzoic acids (PPA*m* or PMA*m* of different molecular weights), where *m* is the repeat

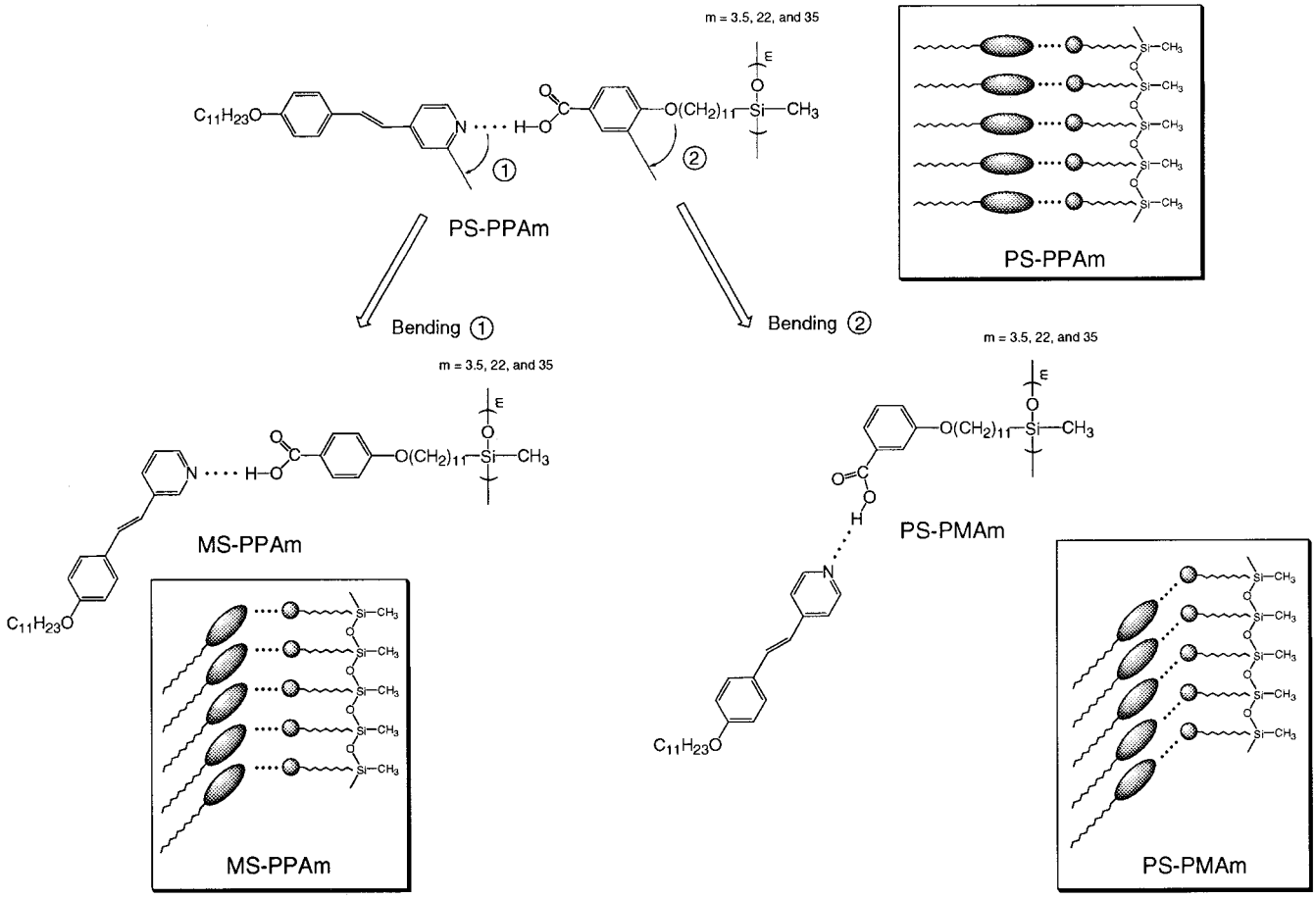

Figure 2. Kinked hydrogen-bonded complexes (monomer−polymer) bending at different sites.

unit of the polysiloxanes, i.e., $m = 3.5$ (or 3−4), 22, and 35. Instead of monomeric acids **8** and **9** (PA and MA), proton donor polymers **10** and **11** (PPA*m* and PMA*m*) are complexed either with stilbazoles (**4** or **6**) or with their analogous *N*-oxides (**5** or **7**) to form supramolecular side-chain polymers (monomer−polymer complexes, i.e., PS−PPA*m*, PS−PMA*m*, MS−PPA*m*, PSO−PPA*m*, PSO−PMA*m*, and MSO−PPA*m*). Some possible arrangements of these monomer−polymer complexes are shown in Figure 2. Consequently, the supramolecular monomer−monomer and monomer−polymer complexes will be compared for the effect of binding kinked hydrogen-bonded pendant groups on the polysiloxane backbones. Accordingly, altering the bending sites of the supramolecular polymers is systematically used to analyze the mesogenic behavior of the kinked hydrogen-bonded side-chain polymers, which enables us to visualize the role of hydrogen bonds in the kinked structures of the supramolecular side-chain polymers.

4 (PS) **5 (PSO)** **6 (MS)** **7 (MSO)** **8 (PA)** **9 (MA)** **10 (PPAm)** **11 (PMAm)**

Experimental Section

Characterization. The ^{1}H and ^{13}C NMR spectra were recorded on a Bruker MSL 200 or 300 spectrometer (200M or 300M Hz) from a $CDCl_3$ or DMSO solution with TMS as the internal standard. The elemental analyses were carried out by Perkin-Elmer 2400 CHN type. The thermal transition temperatures and textures of all products were obtained from Perkin-Elmer DSC-7 and Leitz Laborlux S polarizing optical microscope (POM) equipped with a THMS-600 heating stage. The heating and cooling rates were 10 °C/min for all measurements unless mentioned. Powder X-ray diffraction (XRD) patterns were obtained from an X-ray diffractometer Siemens D-5000 (40 kV, 30 mA) fitted with a temperature controller TTK450. Nickel-filtered Cu Kα radiation was used as an incident X-ray beam.

Synthesis. Preparation of Polysiloxanes Containing 4(or 3)-(Undecyloxy)benzoic Acid 10 or 11 (PPA*m* or PMA*m*). Polysiloxanes containing 4(or 3)-(undecyloxy)benzoic acid (PPA*m* or PMA*m* of different molecular weights), where *m* is the repeat unit of the polysiloxanes, i.e., $m = 3.5$ (or 3−4), 22, and 35, were prepared according to the literature.[10] The whole synthetic route for polysiloxanes containing 4(or 3)-(undecyloxy)benzoic acid is shown in Scheme 1. The detailed syntheses of intermediates and final products are described as follows:

Synthesis of ω-(Undecylenyloxy)benzoic Acids 12. Hydroxybenzoic acid (5 g, 36 mmol) and KOH (5 g, 90 mmol)

Scheme 1. Synthetic Route for Polysiloxanes Containing 3(or 4)-(Undecyloxy)benzoic Acid

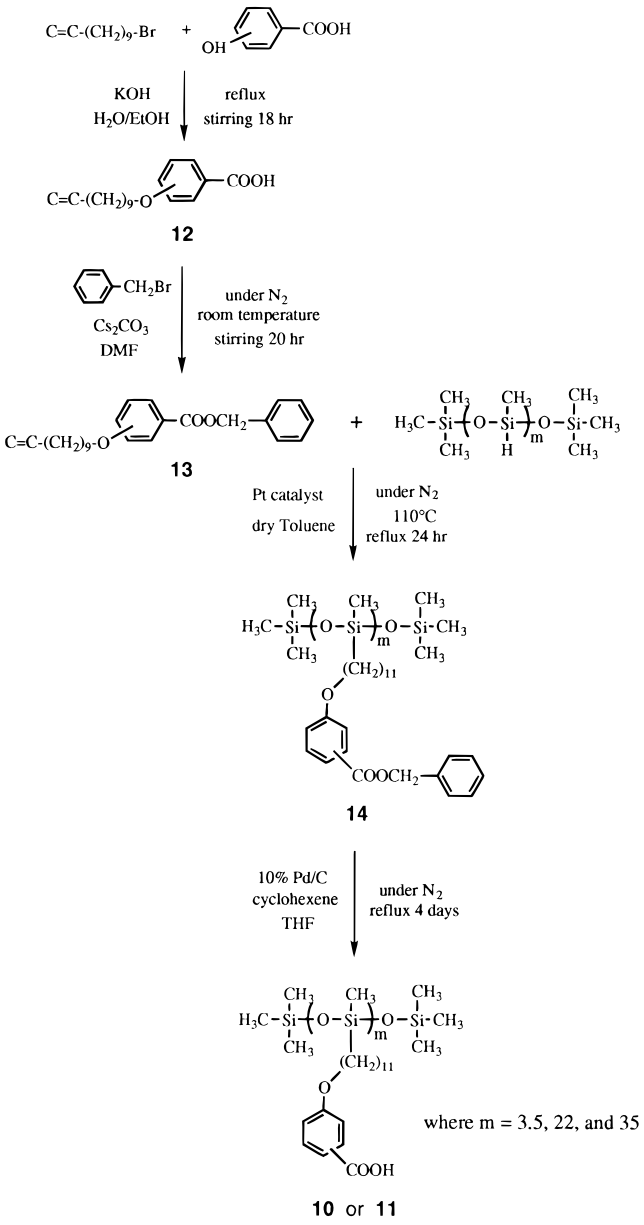

were dissolved in ethanol−water (200 mL, 9:1) and stirred for 20 min. ω-Undecylenyl bromide (16 g, 72 mmol) was then added and the mixture was refluxed for 15 h. When the reaction was completed, KOH (2 g, 36 mmol) was added again and the mixture was refluxed for 3 h. The ethanol was removed from the mixture by evaporation, and the mixture was poured over water and acidified to approximately pH = 5 with concentrated HCl. The precipitate was filtered off and washed with water and hexane. Finally, the precipitate was recrystallized from hexane. Yield: 85−90%.

4-(9-Decenyloxy)benzoic Acid. ^{1}H NMR, δ (DMSO-d_6, ppm): 1.25−1.31 (m, 12H, 6 × CH_2), 1.70 (m, 2H, OCH_2CH_2), 1.97 (m, 2H, =$CHCH_2$), 4.00 (t, 2H, OCH_2, J = 6.38 Hz), 4.95 (m, 2H, CH_2=), 5.74 (m, 1H, =CH), 6.98 (d, 2H, J = 7.35 Hz, Ar−H), 7.86 (d, 2H, J = 7.01 Hz, Ar−H), 12.55 (s, 1H, COOH). ^{13}C NMR, δ (DMSO-d_6, ppm): 25.37, 28.22, 28.47, 28.65, 28.73, 28.88, 33.12, 67.71, 114.14, 114.55, 122.73, 131.27, 138.77, 162.25, 166.92. Anal. Calcd for $C_{18}H_{26}O_3$: C, 74.45; H, 9.02. Found: C, 74.20; H, 9.10.

3-(9-Decenyloxy)benzoic Acid. ^{1}H NMR, δ (DMSO-d_6, ppm): 1.24 (m, 12H, 6 × CH_2), 1.69 (m, 2H, OCH_2CH_2), 1.97 (m, 2H, =$CHCH_2$), 3.96 (m, 2H, OCH_2), 4.92 (m, 2H, CH_2=), 5.76 (m, 1H, =CH), 7.13−7.98 (m, 4H, Ar−H), 12.90 (s, 1H, COOH). ^{13}C NMR, δ (DMSO-d_6, ppm): 25.41, 28.24, 28.55, 28.74, 33.13, 67.57, 114.45, 119.10, 121.36, 129.50, 132.12, 138.70, 158.61, 167.06. Anal. Calcd for $C_{18}H_{26}O_3$: C, 74.45; H, 9.02. Found: C, 74.44; H, 9.06.

Synthesis of Benzyl ω-Undecylenyloxy Benzoates 13. The desired ω-(undecylenyloxy)benzoic acid prepared above (32 mmol) was dissolved in 100 mL of dry DMF under a N_2 atmosphere at room temperature, and 25 mmol of Cs_2CO_3 was added. After 20 min of stirring at room temperature, 35 mmol of benzyl bromide was added in turn. The resulting mixture was stirred for 20 h at room temperature. After removing the solvent, the rest was extracted with $CHCl_3$. The organic layer was washed with aqueous 5% $NaHCO_3$ and later washed with aqueous saturated NaCl, and then dried over anhydrous $MgSO_4$. Remaining traces of acid were removed by passing the product through a short silica gel column using CH_2Cl_2/hexane (3:1) as eluent. Yield: 80−85%.

Benzyl 4-(9-Decenyloxy)benzoate. ^{1}H NMR, δ ($CDCl_3$, ppm): 1.28−1.38 (m, 12H, 6 × CH_2), 1.74 (m, 2H, OCH_2CH_2), 2.03 (m, 2H, =$CHCH_2$), 3.90 (t, 2H, OCH_2, J = 6.43 Hz), 4.96 (m, 2H, CH_2=), 5.29 (s, 2H, $C_6H_5CH_2$), 5.82 (m, 1H, =CH), 6.86 (d, 2H, J = 7.32 Hz, Ar−H), 7.26−7.41 (m, 5H, Ar−H), 8.02 (d, 2H, J = 7.39 Hz, Ar−H). ^{13}C NMR, δ ($CDCl_3$, ppm): 25.78, 28.72, 28.91, 29.16, 29.23, 29.30, 33.60, 66.03, 67.90, 113.85, 114.00, 122.08, 127.82, 128.29, 131.48, 136.19, 138.81, 162.84, 165.81. Anal. Calcd for $C_{25}H_{33}O_3$: C, 78.91; H, 8.48. Found: C, 78.70; H, 8.58.

Benzyl 3-(9-Decenyloxy)benzoate. ^{1}H NMR, δ ($CDCl_3$, ppm): 1.30−1.44 (m, 12H, 6 × CH_2), 1.77 (m, 2H, OCH_2CH_2), 2.05 (m, 2H, =$CHCH_2$), 4.02 (t, 2H, OCH_2, J = 6.43 Hz), 4.95 (m, 2H, CH_2=), 5.34 (s, 2H, $C_6H_5CH_2$), 5.85 (m, 1H, =CH), 7.09 (m, 1H, Ar−H), 7.27−7.44 (m, 5H, Ar−H), 7.63 (m, 3H, Ar−H). ^{13}C NMR, δ ($CDCl_3$, ppm): 25.93, 28.84, 29.10, 29.32, 33.71, 66.62, 68.11, 114.07, 114.87, 119.79, 121.81, 128.07, 128.49, 129.25, 131.29, 136.00, 139.07, 159.06, 166.25. Anal. Calcd for $C_{25}H_{33}O_3$: C, 78.91; H, 8.48. Found: C, 78.52; H, 8.58.

Synthesis of Polysiloxanes with Benzyl Protecting Group 14. Benzyl ω-undecylenyloxy benzoate (11 mmol) was dissolved in 100 mL of dry, freshly distilled toluene together with the poly(methylhydrosiloxane)s of different molecular weights (10 mmol of SiH group). The poly(methylhydrosiloxane)s were purchased from United Chemical Technologies, Inc. (where the repeat units of the polysiloxanes are 3.5, 22, and 35). The reaction mixture was heated to 110 °C under a N_2 atmosphere and 100 μg of (divinyltetramethyldisiloxane)-platinum catalyst (also purchased from United Chemical Technologies, Inc.) was injected with a syringe as a solution in toluene (1 mg/mL). The reaction mixture was refluxed (110 °C) under a N_2 atmosphere. The reaction was monitored by observing the disappearance of the Si−H stretching at 2160 cm^{-1} in the FTIR spectrum. FTIR spectra of the reaction mixture were run on sodium chloride disks. After cooling, the reaction mixture was concentrated, and the excess of benzyl ω-undecylenyloxy benzoates was separated from polysiloxane by passing the reaction mixture through a flash silica gel column using CH_2Cl_2/hexane (2:1) as eluent. The polysiloxane was then eluted from the column using tetrahydrofuran. A highly viscous liquid was obtained after removing tetrahydrofuran. Yield: 80−85%.

Synthesis of Polysiloxanes Containing 4(or 3)-(Undecyloxy)benzoic Acid 10 or 11 (PPA*m* or PMA*m*). The following is a typical procedure for the removal of benzyl protecting groups from polysiloxane. A solution of 0.5 g of polysiloxane in a mixture of 25 mL of THF and 5 mL of EtOH containing 0.2 g of 10% Pd/C was degassed for 1 h. Then 15 equiv of distilled cyclohexene was added, and the mixture was boiled for 4 days under a N_2 atmosphere. After cooling, the reaction mixture was filtered through Celite, and the filtrate was concentrated and precipitated into hexane. The resulting white solid was washed with hexane and recrystallized from ethanol and dried under vacuum at 60 °C for 15 h. Yield: 85−90%. The calculated molecular weights of all PPA*m* and PMA*m* after the complete hydrosilylation reaction of poly(methylhydrosiloxane) with the olefin (ω-(undecylenyloxy)-

benzoic acid) were confirmed by GPC. The NMR results (^{1}H NMR spectra) of PPA*m* and PMA*m* are shown as follows:

PPA3.5. ^{1}H NMR, δ (DMSO-d_6, at 67 °C, ppm): 0.07 (Si-(CH_3)O), 0.52 (Si$(CH_3)O_2$), 1.26, 1.69 (CH_2), 3.99 (OCH_2), 6.91, 7.87 (Ar−H).

PPA22. ^{1}H NMR, δ (DMSO-d_6, at 67 °C, ppm): 0.03 (Si-(CH_3)O), 0.49 (Si$(CH_3)O_2$), 1.21, 1.62 (CH_2), 3.90 (OCH_2), 6.85, 7.82 (Ar−H).

PPA35. ^{1}H NMR, δ (DMSO-d_6, at 67 °C, ppm): 0.02 (Si-(CH_3)O), 0.49 (Si$(CH_3)O_2$), 1.21, 1.62 (CH_2), 3.90 (OCH_2), 6.85, 7.82 (Ar−H).

PMA3.5. ^{1}H NMR, δ (DMSO-d_6, at 67 °C, ppm): 0.04 (Si-(CH_3)O), 0.48 (Si$(CH_3)O_2$), 1.23, 1.66 (CH_2), 3.93 (OCH_2), 7.05−7.50 (Ar−H).

PMA22. ^{1}H NMR, δ (DMSO-d_6, at 67 °C, ppm): 0.02 (Si-(CH_3)O), 0.48 (Si$(CH_3)O_2$), 1.20, 1.62 (CH_2), 3.80 (OCH_2), 7.27−7.47 (Ar−H).

PMA35. ^{1}H NMR, δ (DMSO-d_6, at 67 °C, ppm): 0.01 (Si-(CH_3)O), 0.50 (Si$(CH_3)O_2$), 1.22, 1.62 (CH_2), 3.90 (OCH_2), 6.98−7.46 (Ar−H).

Synthesis of Stilbazoles and Their *N*-oxides. Stilbazoles and their *N*-oxides (H-bonded acceptors) were prepared according to the literature.[35,36] The results of their ^{1}H and ^{13}C NMR spectra and elemental analyses are as follows:

***trans*-4-(Undecyloxy)-4′-stilbazole 4 (PS).** ^{1}H NMR, δ ($CDCl_3$, ppm): 0.88 (t, 3H, CH_3), 1.27−1.83 (m, 18H, 9 × CH_2), 3.99 (t, 2H, OCH_2), 6.87 (d, 1H, J =16.30 Hz, CH=), 6.91 (d, 2H, J = 8.75 Hz, 2 × Ar−H), 7.27 (d, 1H, J = 16.31 Hz, CH=), 7.34 (s, 2H, 2 × Ar−H), 7.47 (d, 2H, J = 8.78 Hz, 2 × Ar−H), 8.55 (s, 2H, 2 × Ar−H). ^{13}C NMR, δ ($CDCl_3$, ppm): 14.09, 22.67, 26.02, 29.22, 29.33, 29.37, 29.58, 31.90, 68.16, 114.88, 120.73, 123.28, 128.31, 128.67, 133.44, 146.85, 149.34, 159.96. Anal. Calcd for $C_{24}H_{33}NO$: C, 82.06; H, 9.47; N, 3.99. Found: C, 81.99; H, 9.46; N, 4.03.

***trans*-4-(Undecyloxy)-3′-stilbazole 6 (MS).** ^{1}H NMR, δ ($CDCl_3$, ppm): 0.88 (t, 3H, CH_3), 1.27−1.83 (m, 18H, 9 × CH_2), 3.98 (t, 2H, OCH_2), 6.90 (d, 2H, J =8.75 Hz, 2 × Ar−H), 6.92 (d, 1H, J = 16.14 Hz, CH=), 7.12 (d, 1H, J = 16.47 Hz, CH=), 7.26−7.29 (m, 1H, Ar−H), 7.46 (d, 2H, J = 8.68 Hz, 2 × Ar−H), 7.82 (d, 1H, J =7.85 Hz, Ar−H), 8.45 + 8.69 (2s, 2H, 2 × Ar−H). ^{13}C NMR, δ ($CDCl_3$, ppm): 14.11, 22.67, 26.02, 29.23, 29.33, 29.39, 29.58, 31.90, 68.12, 114.81, 122.07, 123.74, 128.00, 129.03, 130.95, 132.05, 147.12, 147.42, 159.47. Anal. Calcd for $C_{24}H_{33}NO$: C, 82.06; H, 9.47; N, 3.99. Found: C, 81.90; H, 9.47; N, 3.85.

***trans*-4-(Undecyloxy)-4′-stilbazole *N*-oxide 5 (PSO).** ^{1}H NMR, δ ($CDCl_3$, ppm): 0.88 (t, 3H, CH_3), 1.27−1.83 (m, 18H, 9 × CH_2), 3.99 (t, 2H, OCH_2), 6.86 (d, 1H, J = 16.29 Hz, CH=), 6.91 (d, 2H, J = 8.74 Hz, 2 × Ar−H), 7.12 (d, 1H, J = 16.30 Hz, CH=), 7.33 (d, 2H, J = 7.20 Hz, 2 × Ar−H), 7.45 (d, 2H, J = 8.73 Hz, 2 × Ar−H), 8.14 (d, 2H, J = 7.19 Hz, 2 × Ar−H). ^{13}C NMR, δ ($CDCl_3$, ppm): 14.09, 22.66, 26.01, 29.19, 29.31, 29.58, 31.89, 68.11, 114.72, 120.98, 122.68, 123.77, 125.95, 128.70, 130.02, 134.97, 138.76, 159.32. Anal. Calcd for $C_{24}H_{33}NO_2$: C, 78.42; H, 9.06; N, 3.81. Found: C, 77.97; H, 8.99; N, 3.75.

***trans*-4-(Undecyloxy)-3′-stilbazole *N*-oxide 7 (MSO).** ^{1}H NMR, δ ($CDCl_3$, ppm) 0.88 (t, 3H, CH_3), 1.27−1.82 (m, 18H, 9 × CH_2), 3.98 (t, 2H, OCH_2), 6.76 (d, 1H, J = 18.40 Hz, CH=), 6.91 (d, 2H, J = 8.65 Hz, 2 × Ar−H), 7.11 (d, 1H, J = 16.29 Hz, CH=), 7.20−7.27 (m, 1H, Ar−H), 7.36 (d, 1H, J = 8.01 Hz, Ar−H), 7.44 (d, 2H, J =8.67 Hz, 2 × Ar−H), 8.07 (d, 1H, J = 6.56 Hz, Ar−H), 8.33 (s, 1H, Ar−H). ^{13}C NMR, δ ($CDCl_3$, ppm): 14.08, 22.66, 25.99, 29.17, 29.35, 29.54, 29.58, 31.87, 68.14, 114.88, 119.53, 124.05, 125.74, 128.07, 128.41, 133.52, 136.83, 136.93, 137.45, 160.05. Anal. Calcd for $C_{24}H_{33}NO_2$: C, 78.42; H, 9.06; N, 3.81. Found: C, 77.94; H, 9.10; N, 3.65.

4-(Undecyloxy)benzoic Acid 8 (PA). ^{1}H NMR, δ ($CDCl_3$, ppm): 0.88 (t, 3H, CH_3), 1.27−1.45 (m, 16H, 8 × CH_2), 1.74−1.84 (quint, 2H, 2 × CH_2), 4.02 (t, 2H, OCH_2), 6.93 (d, 2H, J = 8.84 Hz, 2 × Ar−H), 8.05 (d, 2H, J = 8.81 Hz, 2 × Ar−H). ^{13}C NMR, δ ($CDCl_3$, ppm): 14.09, 22.67, 25.96, 29.08, 29.32, 29.34, 29.54, 29.60, 31.89, 68.29, 114.19, 121.34, 132.32, 163.09, 165.24, 171.77, 185.75. Anal. Calcd for $C_{18}H_{28}O_3$: C, 73.93, H, 9.65. Found: C, 73.95, H, 9.66.

Table 1. Phase Transition Temperatures (°C)[a] and Corresponding Enthalpies (J/g), in Parentheses, of Constituents of Hydrogen-Bonded Complexes, i.e., 3(or 4)-(Undecyloxy)benzoic Acid (PA or MA), *trans*-4-(Undecyloxy)-3′(or 4′)-stilbazole (PS or MS), and Their *N*-Oxide Derivatives (PSO or MSO)

PA	K	36.4 (70.0)	95.5 (186.1) Sx	66.1 (33.9)	Sx′	80.2 (49.8)	Sc	122.9 (12.8)	126.3 (12.5) N 135.5 (31.2) 128.2 (29.2) I
MA	K	72.3 (95.9)	87.4 (103.0)						I
PS	K	67.7 (114.4)	85.1 (*b*)	SB		79.4 (39.7)	87.3 (*b*)		I
PSO	K	60.2 (85.0)	107.6 (92.9)				SA	131.9 (10.7)	134.8 (10.8) I
MS	K	71.5 (102.2)	Sx	73.2 (39.6)	85.0 (140.7)				I
MSO	K	67.0 (27.6)	91.9 (63.7) Sx	77.9 (39.2)	96.6 (13.6)		SA	114.6 (10.6)	117.2 (9.1) I

[a] Abbreviations: K = crystalline phase, S_X and $S_{X'}$ = unidentified smectic phases, I = isotropic liquid; the orthogonal smectic A phase was characterized by the focal-conic fan texture coexisting with the homeotropic alignment; the tilted smectic C phase was characterized by the broken focal-conic fan texture coexisting with the schlieren texture; mesophases were characterized through optical microscopy and were also confirmed by X-ray diffraction (XRD). [b] Overlapped peaks and the total enthalpy is 158.6 J/g.

3-(Undecyloxy)benzoic Acid 9 (MA). ^{1}H NMR, δ ($CDCl_3$, ppm): 0.88 (t, 3H, CH_3), 1.27−1.49 (m, 16H, 8 × CH_2), 1.75−1.85 (quint, 2H, CH_2), 4.01 (t, 2H, OCH_2), 7.14 (d, 1H, J = 9.92 Hz, Ar−H), 7.36 (t, 1H, Ar−H), 7.60 (s, 1H, Ar−H), 7.69 (d, 1H, J = 7.45 Hz, Ar−H). ^{13}C NMR, δ ($CDCl_3$, ppm): 14.09, 22.67, 26.01, 29.18, 29.35, 29.59, 31.90, 68.30, 115.11, 120.93, 122.46, 129.45, 130.48, 159.20, 172.10. Anal. Calcd for $C_{18}H_{28}O_3$: C, 73.93; H, 9.65. Found: C, 73.99; H, 9.70.

Preparation of H-Bonded Complexes. Hydrogen-bonded complexes (i.e., PS−PA, PS−MA, MS−PA, PSO−PA, PSO−MA, and MSO−PA monomer−monomer complexes) and hydrogen-bonded side-chain polymers (i.e., PS−PPA*m*, PS−PMA*m*, MS−PPA*m*, PSO−PPA*m*, PSO−PMA*m*, and MSO−PPA*m* monomer−polymer complexes) were prepared by slow evaporation from THF solution containing the mixtures of a 1:1 molar ratio of the H-bonded donor and acceptor moieties, followed by drying in vacuo at 60 °C.

Results and Discussion

Liquid Crystalline Properties and Theoretical Calculations. To investigate the effect of binding kinked hydrogen-bonded pendant groups on the polysiloxane backbones to form supramolecular side-chain LCPs, we first discuss a series of comparative monomer−monomer complexes. Thermal properties of the hydrogen-bonded moieties used in this study, PA, MA, PS, PSO, MS, and MSO (with undecyloxy chain $-OC_{11}H_{23}$), are shown in Table 1. These compounds show different mesogenic properties; for example, PS shows a smectic B phase, PSO and MSO show an enantiotropic smectic A phase, PA possesses nematic and Sc phases, and MA does not show any mesogenic properties. Table 2 and Figure 3 show the thermal properties of these H-bonded monomer−monomer complexes (i.e., PS−PA, PS−MA, MS−PA, PSO−PA, PSO−MA, and MSO−PA), which are different from those of their constituent moieties. For instance, the smectic F phase of PS−PA and smectic A and C phases of PS−MA are different from those of their constituents. These monomer−monomer complexes with analogous alkoxyl chain lengths show similar mesogenic properties as those hydrogen-bonded complexes reported in our previous publication.[33]

Table 2. Phase Transition Temperatures (°C) and Corresponding Enthalpies (J/g), in Parentheses, of Hydrogen-Bonded Complexes, (Monomer−Monomer) 1:1 Molar Ratio from Blending 3(or 4)-(Undecyloxy)benzoic Acid (PA or MA) with *trans*-4-(Undecyloxy)-3′(or 4′)-stilbazole (PS or MS) or with Their *N*-Oxide Derivatives (PSO or MSO)

PS-PA	K	100.1 (107.4) / 91.2 (107.2)	SF	122.4 (8.2) / 119.3 (10.1)	Sc	153.1 (30.8) / 149.8 (29.5)			I
PS-MA	K	54.5 (56.9) / 21.0 (23.8)	Sx	36.1 (4.7)	Sc	68.7 (3.4) / 67.0 (*a*)	SA	85.8 (6.4) / 82.8 (*a*)	I
MS-PA	K	81.4 (135.0) / 71.5 (122.9)							I
PSO-PA	K	101.2 (87.8) / 90.6 (*b*)	Sx	107.5 (104.1) / 95.7 (*b*)	Sc		SA	127.1 (14.8) / 124.6 (14.9)	I
PSO-MA	K	54.6(41.7) / 37.3(38.5)[c]					SA	62.5 (11.3) / 60.0 (3.4)	I
MSO-PA	K	111.0 (115.7) / 89.7 (97.0)			Sc	97.0 (*d*)	SA	101.2 (*d*)	I

[a] Overlapped peaks and the total enthalpy is 11.8 J/g. [b] Overlapped peaks and the total enthalpy is 168.7 J/g. [c] Recrystallization peak was observed in the DSC heating scan. [d] Overlapped peaks and the total enthalpy is 16.2 J/g.

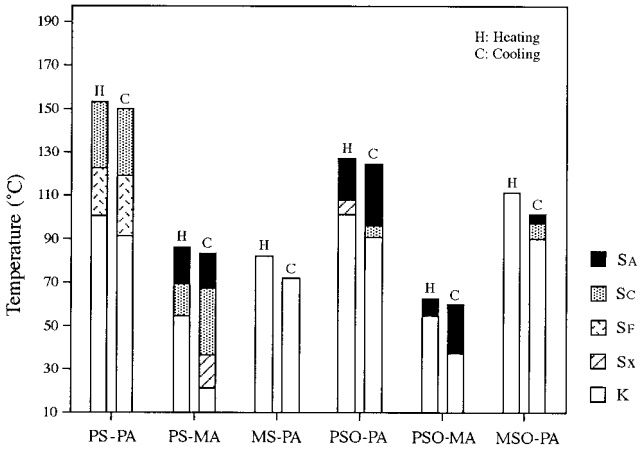

Figure 3. Phase transition temperatures of hydrogen-bonded complexes (monomer−monomer).

Thermal properties of mesogens are often discussed in terms of their molecular shapes. In our H-bonded complexes, it is of interest to know the possible binding geometry of the H-bonded region in order to speculate on the shapes of the complexes. To estimate the binding structures and strength of the H-bonded region, we use pyridine, pyridine *N*-oxide, and formic acid as models of proton acceptors and donor to carry out quantum mechanical calculations. These model compounds in theoretical calculations contain the same H-bonded functional groups as the real mesogens in experiments. Figure 4 shows the optimized binding geometries at the HF/6-31G* level of complexes formed by pyridine···formic acid and pyridine *N*-oxide···formic acid.[37] It is found that introducing an oxide to the mesogen unit has not only enhanced the polarity of the pyridine ring (dipole moment of pyridine at the HF/6-31G* level, 2.31 D; pyridine *N*-oxide, 5.24 D) but has also influenced the ideal pattern of binding geometry. For the pyridine···formic acid complex, a linear N···H−O hydrogen bond, almost collinear with the C_2 axis of pyridine, is accompanied by a very weak C−H···O interaction (Figure 4a).[38,39] Both H's involved in binding are in the direction of lone pairs of N and O heteroatoms. For the pyridine *N*-oxide···formic acid complex, the H's involved in binding are also in the direction of lone pairs of hydrogen acceptors, O, and the angle of the major hydrogen bond O···H−O is also close to linearity (Figure 4b). However, the lone pair of O of the oxide is not collinear with the molecular C_2 axis, therefore, unlike in the pyridine···formic acid complex, the major hydrogen bond O···H−O makes an angle of ca. 130° to the C_2 axis of pyridine *N*-oxide. Conceivably, this difference in binding geometries will induce different extent of bending in the core part. It is also noteworthy that the O···H distances in the O···H−O and C−H···O interactions of the pyridine *N*-oxide complex are significantly shorter than those of the corresponding N···H−O and C−H···O interactions in the pyridine complex. This is because the oxide group is a better hydrogen acceptor and it polarizes the neighboring C−H bond more than the N in pyridine. The stronger polarization effect of the oxide group is revealed by the Mulliken charge of *ortho* H of pyridine *N*-oxide (0.26) and that of pyridine (0.20). Therefore, the combination of O···H−O and C−H···O interactions afford a strong binding (−13.6 kcal/mol) in the oxide complex, which is of comparable strength to that of a doubly hydrogen-bonded formic acid dimer (−12.9 kcal/mol). It should be pointed out that the C−H···O interaction is playing a significant role in the above calculated oxide complex. To simulate the possible case where the N→O···H−O is collinear to achieve better packing, the binding energy of pyridine *N*-oxide···formic acid is calculated with the constraint of linear N→O···H−O. The binding energy thus obtained, −7.7 kcal/mol, is of similar magnitude to that of pyridine···formic acid (−8.9 kcal/mol). Consequently, if the reduction in binding strength of hydrogen bonds can be compensated by better packing interactions, collinear N→O···H−O hydrogen bond is feasible, which is manifested by the experimental data of the monomer−polymer complexes PSO−PMA*m* (shown in the following section).

When stilbazoles (PS and MS) and benzoic acids (PA and MA) are arranged in the binding pattern found for the pyridine···formic acid model system, the idealized core parts of PS−PA and PS−MA are rather linear (Figure 5a,b) and that of MS−PA possesses a distinct bend (Figure 5c). If MS−PA were to become linear for better packing, the strong interaction between N···H−O would have to be sacrificed. The effect of core bending on structures is reflected in the clearing temperatures, *d* spacing values, the mesomorphic phases, and the deviation of clearing temperatures from the theoretical clearing temperatures (discussed below). Similarly, stilbazole *N*-oxides (PSO and MSO) and benzoic acids (PA and MA) are arranged in the binding pattern found for pyridine *N*-oxide···formic acid. It can be seen in Figure 6 that the idealized core parts of PSO−PA and PSO−MA are bent (Figure 6a,b), whereas that of MSO−PA (Figure 6c) is relatively linear among these three oxide complexes. For PSO−PA and PSO−MA, deviation from the idealized bent complexation geometries for better core−core packing is possible, due to the position of the major O···H−O interaction. On the basis of the lower clearing temperature and smaller *d* spacing of PSO−PA relative to those of PS−PA, we believe that the *N*-oxide group indeed introduces some bend to the core region. This conclusion is reinforced by the observation that the clearing temperature (the deviation of clearing temperatures) of PSO−MA is also lower than that of PS−MA (detailed discussion is given later).

In light of the calculation results, it helps us to relate the liquid crystalline properties of the supramolecules, i.e., hydrogen-bonded monomer−monomer and mono-

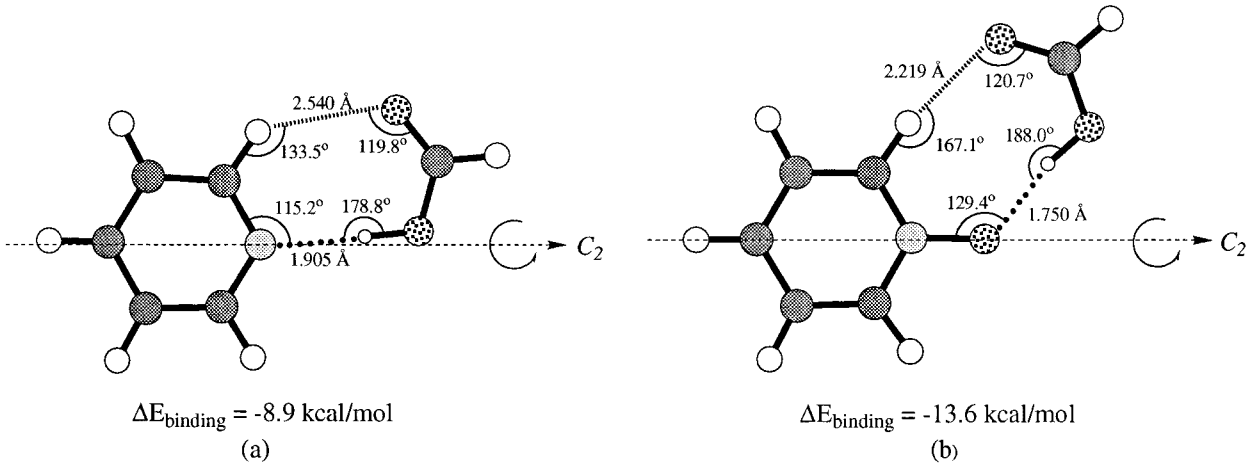

Figure 4. Binding energies and geometries calculated at the HF/6-31G* level for (a) pyridine···formic acid and (b) pyridine *N*-oxide···formic acid. The traditional hydrogen bonds (N···H−O or N→O···H−O) are marked with ··· (dot) lines, and the weaker C−H |||| O hydrogen bonds are marked with |||| (vertical dash) lines. The C_2 axis of pyridine and pyridine *N*-oxide is also shown.

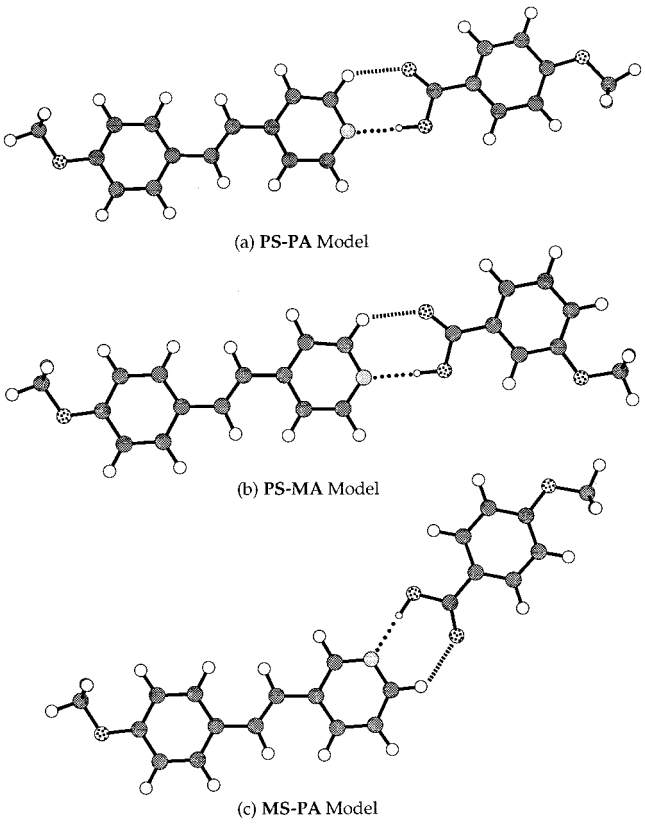

Figure 5. Approximated complexation geometries of (a) PS−PA, (b) PS−MA, and (c) MS−PA models based on calculated geometric features of pyridine···formic acid. (Only one of the most linear geometry is shown for each complex. Due to the position of the major H-bond (represented by ···), it should be easier for PS−PA and PS−MA to adjust the binding geometry in accordance with packing needs. For MS−PA, a more linear binding geometry will sacrifice to the major H-bond to a further extent than that in PS−PA and PS−MA.)

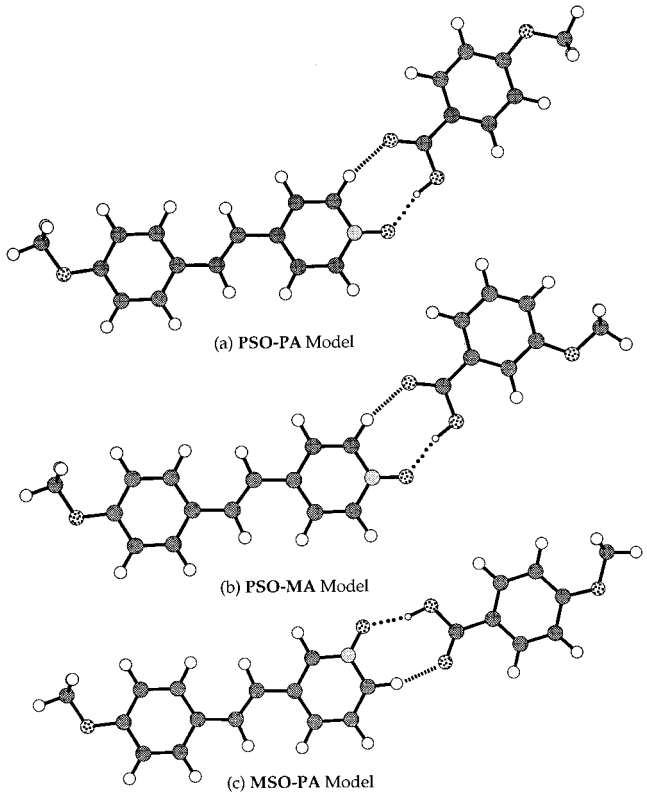

Figure 6. Approximated complexation geometries of (a) PSO−PA, (b) PSO−MA, and (c) MSO−PA models based on calculated geometric features of pyridine *N*-oxide···formic acid. (Only one of the most linear geometry is shown for each complex.)

mer−polymer complexes, to the molecular shapes, which will be considered in the following discussion. On the basis of Table 2 and Figure 3, the PS−PA system has the highest phase transition temperatures (e.g., the S_C phase transition and isotropization temperatures) in all monomer−monomer complexes due to its most linear shape. PSO−PA has the highest isotropization temperature in the comparable *N*-oxide series, because of the flexibility in the H-bonded area it may be less kinked than that drawn in Figure 6a. Owing to its higher flexibility of hydrogen bonding in N→O···H−O, it is possible to have a less kinked shape and become more stable than MSO−PA, which can be further proved in the clearing temperature and XRD measurements. Another interesting result is that *N*-oxide supramolecules show lower isotropization temperatures than their non-oxide analogues, except MSO−PA. This may be deduced from the fact that angular *N*-oxide supramolecular cores are more kinked due to the insertion of the oxygen atom into the hydrogen bond, except that the higher isotropization temperature of MSO−PA may be caused by a more linear structure (Figure 6c) compared with that of MS−PA (Figure 5c).

Interestingly, some kinked structures exhibit mesogenic phases that are not observed in their comparable linear structures. For example, kinked PS−MA possesses an enantiotropic S_A phase, whereas the linear structure of PS−PA does not possess any S_A phase. An enantiotropic S_C phase is introduced in PS−MA (kinked between the core and the flexible part, Figure 5b), even though neither constituent (MA and PS) possesses a S_C phase (Tables 1 and 2). On the other hand, the S_C phase does not exist in MS−PA (kinked in the rigid core bearing H-bonding, Figure 5c), though its constituent PA exhibits a S_C phase. It may be inferred that the S_C phase is more favored in a supramolecular architecture with the kink in the flexible part than that with the kink in the rigid core, yet some kinked structures in the core, e.g., five-membered heterocyclic rings, as well as in aliphatic linkage favor the occurrence of a S_C phase.[34,40−43] Furthermore, the MS−PA system shows the worst mesomorphic behavior in all monomer−monomer complexes (Figure 3). The kink in the angular hydrogen-bonded mesogen of MS−PA (shown in Figure 5) may be detrimental to the formation of the mesophase. Parallel to corresponding systems of stilbazole complexes, the bending of the soft parts of *N*-oxide complexes significantly changes the liquid crystal properties of PSO−MA (Table 2 and Figure 3). In the other *N*-oxide series, the MSO−PA system exhibits a monotropic S_C phase but the PSO−MA system (kinked in both the rigid core by insertion of the oxygen atom into the hydrogen bond and the flexible part in Figure 6b) does not show the S_C phase. In addition, only the MSO−PA system shows both monotropic S_A and S_C phases during the cooling process, so the monotropic phenomena are favored in this special bending supramolecular structure. To consider if the mesomorphism can be preserved in angular supramolecules for the kink moving two rings away from the H-bond, 1:1 complexes of *trans*-3-alkoxy-3′(or 4′)-stilbazoles (or their analogous *N*-oxides) and 3(or 4)-(decyloxy)benzoic acid (for instance kinked complexes formed between *trans*-3-alkoxy-4′-stilbazoles and 4-(decyloxy)benzoic acid) were prepared.[33] Their mesogenic properties are much worse than previous supramolecules; i.e., no S_A and S_C phases were observed. This indicates that if the bending site moves far away from the H-bond, the angular mesogenic packing efficiency will not be recovered easily through the flexible H-bond. Therefore, it shows that kinked supramolecules can sustain better mesomorphism with bending positions near the hydrogen bond.

Compared with the proton donor PA in Table 1, the proton donor polymer PPA*m* exhibits very different mesomorphic behavior. For the pure polymer PPA*m*, no fluid mesomorphic phases have been observed upon heating due to the formation of highly cross-linked ordered structures originated from the intermolecular dimerization of benzoic acids through hydrogen bonding. Tables 3−5 and Figures 7 and 8 show the thermal properties of the monomer−polymer complexes (i.e., PS−PPA*m*, PS−PMA*m*, MS−PPA*m*, PSO−PPA*m*, PSO−PMA*m*, and MSO−PPA*m*), which are also different from those of their original moieties and monomer−monomer complexes. For example, the S_A phases of PS−PPA*m*, PS−PMA*m*, and MS−PPA*m* are all different from those of their constituents. Moreover, IR and powder X-ray diffraction (XRD) measurements reveal that the H-bonds have formed in the H-bonded complexes. These monomer−polymer complexes all exhibit a focal-conic texture or a batonet texture upon cooling in the polarizing optical microscope, which is indicative of either a smectic A or a smectic C phase. These results were also confirmed by the powder XRD measurements.

All monomer−polymer complexes have higher isotropization temperatures than their comparable monomer−monomer systems, respectively (Tables 2−5). In addition, both PS−PPA*m* and PSO−PPA*m* systems have higher isotropization temperatures than their comparable non-oxide and *N*-oxide monomer−polymer systems, respectively. The trend of the monomer−polymer systems in isotropization temperatures is similar to that of the monomer−monomer systems (see Figures 3 and

Table 3. Phase Transition Temperatures (°C) and Corresponding Enthalpies (J/g), in Parentheses, of Hydrogen-Bonded Complexes[a] (Monomer−Polymer) from Blending Polysiloxanes Containing 3(or 4)-(Undecyloxy)benzoic Acid (PPA3.5 or PMA3.5)[b] with *trans*-4-(Undecyloxy)-3′(or 4′)-stilbazole (PS or MS) or with Their *N*-Oxide Derivatives (PSO or MSO)

PS-PPA3.5	K	79.2 (15.1) / 66.1 (10.8)	$S_{X'}$	129.7 (5.4) / 126.7 (5.7)	S_C	183.7 (25.1) / 179.0 (23.5)	I	
PS-PMA3.5	K	56.1 (12.7) / 27.3 (13.1)[c]			S_A	117.1 (9.6) / 110.2 (10.7)	I	
MS-PPA3.5	K	73.2 (28.1) / 53.5 (26.6)			S_A	104.3 (2.7) / 98.4 (4.7)	I	
PSO-PPA3.5	K	93.7 (20.8) / 70.6 (22.0)			S_A	165.7 (6.9) / 163.1 (7.4)	I	
PSO-PMA3.5[d]					S_A	105.2 (3.4) / 103.1 (3.6)	I	
MSO-PPA3.5	K	111.2 (28.7) / 71 8 (21.1)			S_A	132.7 (5.1) / 128.4 (6.5)	I	

[a] 1:1 mole ratio of the benzoic acids in the polysiloxanes (repeat unit $m = 3.5$) and the stilbazoles (or its *N*-oxide derivatives). [b] Phase transition temperatures and corresponding enthalpies of PPA3.5 and PMA3.5: (PPA3.5) K 159.0 (4.9) Isotropic 148.5 (7.2) K; (PMA3.5) K 76.8 (22.7) Isotropic 45.7 (16.6) K. For PMA3.5, no crystallization peak was observed in the DSC cooling scan and the recrystallization peak was observed in the heating scan. [c] Recrystallization peak was observed in the DSC heating scan. [d] No crystallization occurs on cooling to 10.0 °C.

Table 4. Phase Transition Temperatures (°C) and Corresponding Enthalpies (J/g), in Parentheses, of Hydrogen-Bonded Complexes[a] (Monomer−Polymer) from Blending Polysiloxanes Containing 3(or 4)-(Undecyloxy)benzoic Acid (PPA22 or PMA22)[b] with *trans*-4-(Undecyloxy)-3′(or 4′)-stilbazole (PS or MS) or with Their *N*-Oxide Derivatives (PSO or MSO)

PS-PPA22	K	78.0 (14.3) / 60.1 (26.5)	S_X	129.9 (4.9) / 125.9 (6.3)	S_C	135.0 (*c*) / 131.0 (*c*)	S_A	187.8 (8.4) / 181.8 (9.1) I
PS-PMA22	K	85.1 (0.4) / 62.6 (0.3)					S_A	114.1 (5.7) / 109.9 (8.2) I
MS-PPA22	K	74.7 (29.9) / 53.5 (25.3)					S_A	103.8 (0.5) / 92.2 (0.5) I
PSO-PPA22	K	92.4 (10.9) / 69.2 (24.4)					S_A	172.8 (3.4) / 164.9 (4.3) I
PSO-PMA22[d]							S_A	111.5 (2.0) / 106.7 (3.0) I
MSO-PPA22	K	99.1 (14.7) / 72.6 (14.0)					S_A	142.4 (1.8) / 135.6 (3.7) I

[a] 1:1 mole ratio of the benzoic acids in the polysiloxanes (repeat unit $m = 22$) and the stilbazoles (or its *N*-oxide derivatives). [b] Phase transition temperatures and corresponding enthalpies of PPA22 and PMA22: (PPA22) K 165.1 (0.8) Isotropic 151.3 (2.4) K; (PMA22) K 79.1 (9.4) Isotropic 56.1 (8.1) K. For PMA22, no crystallization peak was observed in the DSC cooling scan and the recrystallization peak was observed in the heating scan. [c] The enthalpy was too small to be detected by differential scanning calorimetry, and the phase transition temperature was assigned by polarizing optical microscopy. [d] No crystallization occurs on cooling to 10.0 °C.

Table 5. Phase Transition Temperatures (°C) and Corresponding Enthalpies (J/g), in Parentheses, of Hydrogen-Bonded Complexes[a] (Monomer−Polymer) from Blending Polysiloxanes Containing 3(or 4)-(Undecyloxy)benzoic Acid (PPA35 or PMA35)[b] with *trans*-4-(Undecyloxy)-3′(or 4′)-stilbazole (PS or MS) or with Their *N*-Oxide Derivatives (PSO or MSO)

PS-PPA35	K	82.0 (17.6) ⇌ 58.7 (18.3)	Sx	116.3 (2.0) ⇌ 112.7 (1.1)	S_A	186.7 (4.4) ⇌ 179.1 (4.8)	I
PS-PMA35	K	61.5 (1.7) ⇌ 47.3 (1.4)			S_A	119.4 (7.2) ⇌ 115.9 (10.4)	I
MS-PPA35	K	77.0 (34.7) ⇌ 59.0 (37.7)			S_A	104.2 (2.9) ⇌ 94.8 (5.4)	I
PSO-PPA35	K	91.1 (12.8) ⇌ 65.9 (17.6)			S_A	170.3 (2.4) ⇌ 162.1 (4.0)	I
PSO-PMA35[c]					S_A	118.8 (3.7) ⇌ 114.4 (4.8)	I
MSO-PPA35	K	99.1 (11.2) ⇌ 73.3 (14.0)			S_A	137.2 (0.5) ⇌ 131.0 (1.8)	I

[a] 1:1 mole ratio of the benzoic acids in the polysiloxanes (repeat unit $m = 35$) and the stilbazoles (or its *N*-oxide derivatives). [b] Phase transition temperatures and corresponding enthalpies of PPA35 and PMA35: (PPA35) K 162.7 (0.1) Isotropic 151.1 (1.3) K; (PMA35) K 82.5 (20.7) Isotropic 52.6 (15.1) K. For PMA35, no crystallization peak was observed in the DSC cooling scan and the recrystallization peak was observed in the heating scan. [c] No crystallization occurs on cooling to 10.0 °C.

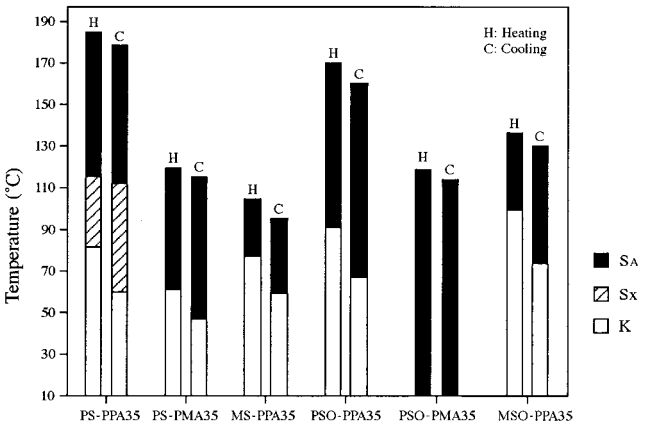

Figure 7. Phase transition temperatures of hydrogen-bonded complexes (monomer−polymer complexes as repeat unit $m = 35$ for polymers).

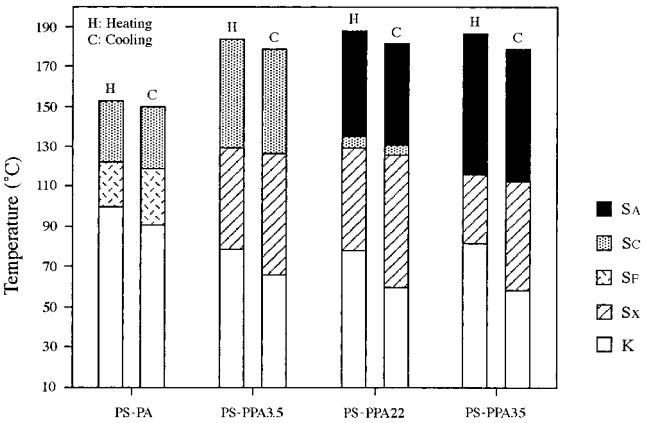

Figure 8. Phase transition temperatures of hydrogen-bonded complexes (monomer−monomer complex and monomer−polymer complexes) with different molecular weights of proton donors.

7). The only difference is that PSO−PMA35 has a higher rank of the isotropization temperature (the fifth rank in Figure 7) in the monomer−polymer complexes than the analogous PSO−MA (the sixth rank in Figure 3) in the monomer−monomer complexes. This result suggests that the N→O···H−O hydrogen bond in the monomer−polymer complexes is liable to sustain a more linear form than the monomer−monomer complexes, such that the C−H···O interaction is less effective in the supramolecular polymers. Another interesting phenomenon is that the enantiotropic S_A phase is more favored in monomer−polymer complexes with higher molecular weights of donor polymers (Tables 2−5 and Figure 8). For instance, PS−PA and PS−PPA3.5 have no S_A phase, PS−PPA22 has a S_A phase and a narrow S_C phase, and PS−PPA35 has only a S_A phase. Significantly, the mesogenic properties of monomer−monomer and monomer−polymer complexes (PS−PA, PS−PPA3.5, PS−PPA22, and PS−PPA35) in Figure 8 show that the larger the molecular weight of PPA*m* in the complexes, the stabler the S_A arrangement and the less stabler the S_C arrangement. This phenomenon may imply that the S_C phase is more preferred in the lower molecular weight forms due to the supramolecular architecture inherited from their analogous monomer−monomer complexes, and the orthogonal S_A arrangement is induced by binding a large number of proton donors onto the backbones of the polymers, where the tilted S_C arrangement is more difficult to be achieved. Besides, in comparison with MS−PA (no mesogenic phases) and MSO−PA (monotropic S_A and S_C phases), MS−PPA*m* and MSO−PPA*m* systems exhibit the enantiotropic S_A phase, which reveal that monomer−polymer complexes possess better mesomorphic behavior than their analogous monomer−monomer complexes. Correspondingly, the stability of the S_A phase can be enhanced in the kinked PS−PMA*m* and PSO−PMA*m* systems and the other phases (Sc, highly ordered Sx, and crystalline phases) are suppressed, which may be also attributed to the polysiloxane backbones stabilizing the assembly of the S_A phase and restricting the tilted Sc and highly ordered Sx packing in the supramolecular polymer form. Hence, through binding the proton donors (acids) to the backbones of the polymers, the S_A phase is favored and stabilized in the supramolecular polymers with or without kinked structures. Another similar result is that *N*-oxide supramolecular polymers show lower isotropization temperatures than their nonoxide analogues, except MSO−PPA*m*. This may be originated from the same reason as their analogous monomer−monomer complexes; i.e., *N*-oxide supramolecular cores are more kinked compared with their nonoxide analogues, except that the higher isotropization temperatures of MSO−PPA*m* may be caused by the more linear structures compared with MS−PPA*m*. Similar to monomer−monomer complexes, the higher isotropization temperatures of MSO−PPA*m* may be also owing to the more linear H-bonded mesogenic cores of MSO−PPA*m* compared with those of PSO−PMA*m*. However, if the deviation of clearing temperatures from the theoretical clearing temperatures are taken into account in monomer−polymer complexes, different results may occur and the detailed discussion will be verified later (in the discussion section of "shape effects on clearing temperatures"). Moreover, MS−PPA*m* (bending in the rigid core bearing H-bonding) does show a narrower S_A phase compared with PS−PMA*m* (bending in the flexible part), so it strongly implies again that a kink in the rigid core bearing H-bonding may suggest the lower stability of the S_A phase.

Table 6. Largest *d* Spacing of Smectic A Phase in Hydrogen-Bonded Complexes (Monomer−Monomer and Monomer−Polymer) Detected by Powder XRD Measurements

complex	*d* spacing (Å) (heating)	complex	*d* spacing (Å) (heating)	complex	*d* spacing (Å) (heating)	complex[e]	*d* spacing (Å) (heating)
PS−PA[a]		PS−PPA3.5[d]		PS−PPA22	45.66 (140 °C)	PS−PPA35	45.04 (120 °C)
PS−MA	38.06 (78 °C)	PS−PMA3.5	44.10 (70 °C)	PS−PMA22	42.65 (87 °C)	PS−PMA35	42.05 (70 °C)
MS−PA[b]		MS−PPA3.5	43.60 (80 °C)	MS−PPA22	42.23 (75 °C)	MS−PPA35	42.73 (80 °C)
PSO−PA	38.69 (110 °C)	PSO−PPA3.5	44.54 (100 °C)	PSO−PPA22	44.38 (95 °C)	PSO−PPA35	44.19 (110 °C)
PSO−MA	38.40 (57 °C)	PSO−PMA3.5	44.49 (50 °C)	PSO−PMA22	43.61 (50 °C)	PSO−PMA35	44.44 (50 °C)
MSO−PA	37.85 (100 °C)[c]	MSO−PPA3.5	43.61 (115 °C)	MSO−PPA22	44.75 (105 °C)	MSO−PPA35	44.53 (115 °C)

[a] No smectic A phase is observed and the largest *d* spacing value in the Sc phase is 38.38 Å. [b] No smectic A phase is observed. [c] Monotropic smectic A phase is observed upon cooling. [d] No smectic A is observed and the largest *d* spacing value in the smectic C phase is 43.56 Å at 130 °C (upon heating). [e] A broad peak centered around $2\theta = 20.5°$ and its corresponding *d* spacing = 4.34 Å in smectic A and C phases.

In general, higher isotropization temperatures and broader mesogenic phases (e.g., S_A phase) may be favored in the monomer−polymer complexes than in the monomer−monomer complexes; furthermore, kinked supramolecular polymers may show new or broader mesogenic phases in comparison with their linear isomeric structures or monomer−monomer complexes.

XRD Measurements. Powder X-ray diffraction (XRD) measurements are useful to prove the smectic layer arrangements and thus the formation of the kinked supramolecular structures. If the S_A phase is assumed to have a more linear structure (especially the largest *d* spacing values of the orthogonal S_A phase were observed at the lowest temperatures of the S_A phase in each heating or cooling cycle) than any other mesophases, it would be considered useful to relate the XRD data to the calculated molecular arrangements in Figures 4−6. Table 6 shows the largest *d* spacing values of the S_A phase that were obtained from the XRD measurements. Since the largest *d* spacing (layer thickness) of the S_A phase (molecule orthogonal to the layer) is correlated to the length of the supramolecule, the degree of the bend may be estimated by the XRD data. Molecular shapes of Figures 5 and 6 calculated by quantum mechanical calculations can also be further confirmed by these XRD results. The lengths of each component calculated by the molecular modeling are listed as PS (or MS) = 24.2−25.9 Å, PSO (or MSO) = 25.6−27.3 Å, PA (or MA) = 19.0−21.2 Å, and PPA*m* (or PMA*m*) = 21.0−23.1 Å, where the latter value is the fully extended molecular length and the former value is the molecular projection length along the rigid core.

In our previous work,[33] it was found that the most linear structure of the monomer−monomer supramolecular systems is CnPS−PA at alkoxy length $n = 8$, where the *d* spacing value is 43.16 Å, and it is much larger than the *d* spacing values (35.49−38.42 Å) of the other kinked systems. With regard to the monomer−polymer systems, Table 6 indicates that all systems are somewhat kinked in shape to similar extent, except for PS−PPA22 and PS−PPA35. Since PS−PA and PS−PPA3.5 in this work do not possess any S_A phase, the largest *d* spacing values in their tilted Sc arrangements are still as large as 38.38 and 43.56 Å, respectively, which are comparable to those of their analogous systems in their longest orthogonal S_A layer *d* spacing forms. Thus, it can be assumed that PS−PA and PS−PPA3.5 systems should have the largest *d* spacing values if they possess the orthogonal S_A phase rather than the tilted Sc phase. For example, the PS−PPA3.5 complex displays the focal-conic texture identified as either a smectic A or a smectic C phase in the beginning. Besides, a broad peak centered around $2\theta = 19-20°$ and its corresponding *d* spacing = 4.4−4.7 Å has been observed in XRD measurements. This indicates that the lateral packing within the smectic layer is disordered and mesogens are separated around 4.6 Å, so a smectic A or a smectic C phase is further confirmed by XRD measurements. However, the distance for Si−O−Si is around 2.4 Å, so it suggests that the pendant groups are possibly antiparallel packed. According to Table 6, the largest *d* spacing value of PS−PPA3.5 is 43.56 Å (at 130 °C upon heating), which is smaller than the S_A *d* spacing values of all other monomer−polymer ($m = 3.5$) complexes in their smectic A phase, e.g., PSO−PPA3.5 (44.54 Å), MS−PPA3.5 (43.60 Å), MSO−PPA3.5 (43.61 Å), PS−PMA3.5 (44.1 Å), PSO−PMA3.5 (44.49 Å). This result suggests that the focal-conic texture in PS−PPA3.5 is suitable to be identified as the tilted smectic C phase by XRD studies. As a whole, the *d* spacing values in Table 6 suggest that all PS−PPA*m* systems have the most linear structures of these supramolecular systems. The small differences in *d* spacing values of these kinked supramolecular polymers also suggest that the degree of the molecular bending is similar in most of the systems, and these kinked supramolecular polymers may have less kinked shapes than those drawn in Figure 2. The similar lengths of these kinked positional isomeric supramolecules in Table 6 may be reasoned by the higher flexibility of the H-bond compared with the covalent bond. These results may infer that the total lengths of the molecular structures are similar in most of the kinked systems, and the hydrogen bonds of various molecular shapes in Figures 5 and 6 must be more flexible than expected.

On the basis of these findings in XRD experiments, various kinked core structures of supramolecules containing *N*-oxides, e.g., PSO−PA, PSO−MA, and MSO−PA systems, are introduced by the insertion of an oxygen atom into the hydrogen bond. This is evidenced by the shorter *d* spacing values and lower clearing temperatures of kinked PSO−PPA*m* systems compared with those of linear PS−PPA*m* systems. Another interesting phenomenon in Table 6 is that all *d* spacing values of PSO−PMA*m* are larger than those of PS−PMA*m*, and all *d* spacing values of MSO−PPA*m* are larger than those of MS−PPA*m*. As described previously, PSO−MA exhibits very different kinked properties depending on the thermal history and the flexible length, i.e., more linear shape observed during repeated cooling cycles and enhanced phenomena observed in PSO−MA systems with longer flexible parts.[33] This is possibly because the kinked PSO−MA could be organized into a more linear form upon cooling from the isotropic state with higher flexibility and mobility. Thus, it reveals that the N→O···H−O hydrogen bond in the monomer−monomer complexes is more flexible and linear than those are drawn in Figure 6. With respect to PSO−PMA*m*, all PSO−

PMA*m* systems show larger *d* spacing values than PS−PMA*m* systems, and this is again due to the more linear shape of PSO−PMA*m* compared with that of PS−PMA*m* (Figures 5 and 6). The N→O···H−O hydrogen bond in the monomer−polymer complexes is prone to maintain a more linear shape, such that the C−H···O interaction is sacrificed in supramolecular polymers. Regarding MSO−PPA*m*, all MSO−PPA*m* systems show larger *d* spacing values than MS−PPA*m* systems, and this is also due to the more linear shape of MSO−PA compared with that of MS−PA (Figures 5 and 6). MSO−PA shows a larger *d* spacing value than MS−PA as well (at alkoxy length $n = 16$ shown in the previous work).[33] These XRD results agree that the insertion of an oxygen atom into the hydrogen bond does change the shapes and thus the lengths of the supramolecules, which also coincides with the theoretical calculation shown in Figures 5 and 6. Judged by the similar *d* spacing values of PSO−PPA*m*, PSO−PMA*m*, and MSO−PPA*m* (Table 6), it seems that the degree of kink in these systems is not very distinct. This may be reasoned by the higher flexibility of the *N*-oxide hydrogen bonds in the supramolecules, which will be further confirmed by the shape effect on the clearing temperature. Overall, the *d* spacing data generally match the calculated molecular lengths of the quantum mechanical calculations.

XRD measurements also prove that some bending structures of monomer−polymer complexes are not so kinked as thought in Figure 2 (see Table 6). In addition, the bending angles of the monomer−polymer complexes are not so large as their analogous monomer−monomer complexes. For example, PSO−PA and PSO−MA have similar S_A *d* spacing values (38.40−38.69 Å) in Table 6, and these values are much smaller than the calculated *d* spacing value (44.6 Å) possessing linear structures. However, their analogous monomer−polymer complexes PSO−PPA*m*, PSO−PMA*m*, and MSO−PPA*m* have much more linear lengths (43.61−44.53 Å) in XRD data, which are comparable with the molecular modeling *d* spacing value (46.6 Å) in a linear shape. In this case, if the monomer−polymer complexes adopt the shapes of their monomer−monomer complexes, then the difference of their largest *d* spacing values in the S_A phase should be around 3.0 Å by calculation (the extra length of $-Si-CH_3$ in monomer−polymer complexes). However, the differences of the *d* spacing values between monomer−monomer complexes and their monomer−polymer complexes are as high as 5.85 Å (in PSO−PPA*m*), 6.9 Å (in MSO−PPA*m*), 6.04 Å (in PS−PMA*m*), and 6.09 Å (in PSO−PMA*m*), respectively, so the more linear configuration in the supramolecular polymers are introduced in these monomer−polymer complexes and it also suggests that these less kinked structures may be deduced from the restriction of the benzoic acids bound through polysiloxane backbones.

It was found that the most linear structure of the monomer−monomer supramolecular systems is PS−PA in our previous communication,[33] and the largest difference of the *d* spacing values between the most linear structure (43.16 Å) and the most kinked structure (35.49 Å) is 7.67 Å. However, in the monomer−polymer supramolecular systems the largest difference of the *d* spacing values between the most linear structure (45.66 Å in PS−PPA22) and the most kinked structure (42.05 Å in PS−PMA35) is only 3.61 Å. Therefore, the monomer−polymer complexes have less molecular length differences in their head-to-tail forms, and most monomer−polymer systems show the S_A phase and have similar *d* spacing values. Nevertheless, this result indicates that all monomer−monomer systems are somewhat kinked in their shape to similar extent, except for PS−PA. Besides, the nonlinearity of the monomer−polymer systems have been compensated by binding these proton donors through polysiloxane backbones. By these XRD measurements and the calculated *d* spacing values, we can conclude that the nonlinearity of the monomer−polymer complexes are not so large as their analogous monomer−monomer complexes. However, the bending arrangements of the hydrogen-bonded cores in monomer−polymer systems are still adopted from their analogous monomer−monomer systems and behave similarly in their isotropization temperatures described below, though their angularity seems to be reduced into a more linear shape (in the head-to-tail aspect) in the monomer−polymer complexes. The explanation for the similar lengths of different supramolecules may be reasoned by the higher flexibility of the hydrogen bond compared with the covalent bond.

Shape Effects on Clearing Temperatures. According to our previous observation, the clearing temperatures (T_c) of the H-bonded complexes are predominantly affected by their shapes, i.e., geometries. Generally, in comparing with the melting temperatures of these hydrogen-bonded complexes, the clearing temperatures of the mixtures are easier to predict from the known data of each component. Therefore, the clearing temperatures (T_c) of the mixtures are able to be reliably obtained as they tend to be linear functions (see eq 1)[44] of T_c's of their constituent components.

$$T_c = \Sigma(T_{ci}X_i) \tag{1}$$

where T_{ci} is the clearing temperature of the component *i* and X_i is the mole ratio of the component *i* in the mixture. Moreover, this relation holds better when compounds of similar polarities are mixed; otherwise, the larger difference in their polarities causes a larger negative deviation from ideal behavior. Since the clearing temperatures (T_{ci}) of all constituent components in our study are very distinct, the experimental T_c (T_2) values of different-shaped complexes with hydrogen-bonded interactions are not suitable to be compared without considering the T_{ci} values of their individual components. To analyze the effect of the hydrogen-bonded complexation, the deviation temperatures (ΔT) of all complexes, i.e., the experimental T_c (T_2) values with hydrogen-bonded interactions minus the theoretical T_c (T_1) values, are required to be compared. Tables 7−10 illustrate the theoretical T_c (T_1) values of the monomer−monomer and monomer−polymer complexes obtained from eq 1, the experimental T_c (T_2) values and the deviation values (ΔT) for all complexes. From the deviation temperatures (ΔT) of these complexes, the effect of the kink in hydrogen-bonded structures can be justifiably examined.

According to Table 7 and Figures 5 and 6 of the monomer−monomer complexes, we can conclude that the deviation temperature (ΔT) has been exclusively enhanced in PS−PA (positive enhancement $\Delta T = 41.7$ °C) resulting from the most linear structure after complex formation through hydrogen bonding. Thus, the length of the rigid core in the monomer−monomer complexes may be enlarged through hydrogen bonding, which may cause the positive effects on the clearing

Table 7. Theoretical Clearing Temperatures (T_1), Experimental Clearing Temperatures (T_2), and Deviation Temperatures ΔT ($T_2 - T_1$) of PS−PA, PS−MA, MS−PA, PSO−PA, PSO−MA, and MSO−PA

complex	T_1 (theor T_c)[a] (°C)	T_2 (exp T_c)[b] (°C)	ΔT ($T_2 - T_1$) (°C)
PS−PA	111.4	153.1	+41.7
PS−MA	87.4	85.8	−1.6
MS−PA	110.3	81.4	−28.9
PSO−PA	135.2	127.1	−8.1
PSO−MA	111.1	62.5	−48.6
MSO−PA	126.4	111.0	−15.4

[a] Theoretical T_c (T_1) is the clearing (isotropization) temperature of the blend without interactions, i.e., $T_1 = T_{c1}X_1 + T_{c2}X_2$, where T_{c1} and T_{c2} are clearing temperatures of the proton donor and proton acceptor, respectively, and X_1 (molar ratio of proton donor) = X_2 (molar ratio of proton acceptor) = 0.5. The isotropization temperatures of proton donors and acceptors are PA (135.5 °C), MA (87.4 °C), PS (87.3 °C), PSO (134.8 °C), MS (85.0 °C), and MSO (117.2 °C). [b] Experimental T_c (T_2) is the clearing (isotropization) temperature of the complex with hydrogen-bonded interactions. [c] ΔT is the deviation temperature of the experimental isotropization temperature (T_2) minus the theoretical isotropization temperature (T_1), i.e., $\Delta T = T_2 - T_1$.

Table 8. Theoretical Clearing Temperatures (T_1), Experimental Clearing Temperatures (T_2), and Deviation Temperatures ΔT ($T_2 - T_1$) of PS−PPA3.5, PS−PMA3.5, MS−PPA3.5, PSO−PPA3.5, PSO−PMA3.5, and MSO−PPA3.5

complex	T_1 (theor T_c)[a] (°C)	T_2 (exp T_c) (°C)	ΔT ($T_2 - T_1$) (°C)
PS−PPA3.5	123.2	183.7	+60.5
PS−PMA3.5	82.1	117.1	+35.0
MS−PPA3.5	122.0	104.3	−17.7
PSO−PPA3.5	146.9	165.7	+18.8
PSO−PMA3.5	105.8	105.2	−0.6
MSO−PPA3.5	138.1	132.7	−5.4

[a] The isotropization temperatures of proton donors and acceptors are PPA3.5 (159.0 °C), PMA3.5 (76.8 °C), PS (87.3 °C), PSO (134.8 °C), MS (85.0 °C), and MSO (117.2 °C).

Table 9. Theoretical Clearing Temperatures (T_1), Experimental Clearing Temperatures (T_2), and Deviation Temperatures ΔT ($T_2 - T_1$) of PS−PPA22, PS−PMA22, MS−PPA22, PSO−PPA22, PSO−PMA22, and MSO−PPA22

complex	T_1 (theor T_c)[a] (°C)	T_2 (exp T_c) (°C)	ΔT ($T_2 - T_1$) (°C)
PS−PPA22	126.2	187.8	+61.6
PS−PMA22	83.2	114.1	+30.9
MS−PPA22	125.1	103.8	−21.3
PSO−PPA22	150.0	172.8	+22.8
PSO−PMA22	107.0	111.5	+4.5
MSO−PPA22	141.2	142.4	+1.2

[a] The isotropization temperatures of proton donors and acceptors are PPA22 (165.1 °C), PMA22 (79.1 °C), PS (87.3 °C), PSO (134.8 °C), MS (85.0 °C), and MSO (117.2 °C).

temperatures, such as PS−PA. However, the other monomer−monomer systems have negative effects on the clearing temperatures due to the different degrees of nonlinearities in the kinked supramolecular structures. For the monomer−polymer complexes (Tables 8−10), PS−PPA*m* systems also have the largest deviation temperatures (positive enhancement ΔT = 60.5, 61.6, and 61.7 °C, respectively) in each series owing to their most linear structures. Nevertheless, the other monomer−polymer complexes have more positive effects on the clearing temperatures than the monomer−monomer complexes since the less kinked structures of the supramolecular polymers are obtained through

Table 10. Theoretical Clearing Temperatures (T_1), Experimental Clearing Temperatures (T_2), and Deviation Temperatures ΔT ($T_2 - T_1$) of PS−PPA35, PS−PMA35, MS−PPA35, PSO−PPA35, PSO−PMA35, and MSO−PPA35

complex	T_1 (theor T_c)[a] (°C)	T_2 (exp T_c) (°C)	ΔT ($T_2 - T_1$) (°C)
PS−PPA35	125.0	186.7	+61.7
PS−PMA35	84.9	119.4	+34.5
MS−PPA35	123.9	104.2	−19.7
PSO−PPA35	148.4	170.3	+21.5
PSO−PMA35	108.7	118.8	+10.1
MSO−PPA35	140.0	137.2	−2.8

[a] The isotropization temperatures of proton donors and acceptors are PPA35 (162.7 °C), PMA35 (82.5 °C), PS (87.3 °C), PSO (134.8 °C), MS (85.0 °C), and MSO (117.2 °C).

binding proton donors onto the backbones of the polymers.

For the non-oxide monomer−monomer complexes, ΔT values are in the following order: PS−PA (the most linear structure; ΔT = +41.7 °C) > PS−MA (kinked between the core and the flexible part; ΔT = −1.6 °C) > MS−PA (kinked in the rigid core bearing the H-bond; ΔT = −28.9 °C). This shows that various nonlinear shapes may be detrimental to the packing of the liquid crystalline or crystalline phases in different ways. For the kinked structures in this series, the molecular structure kinked between the core and flexible part (PS−MA) has a greater tendency to sustain a higher clearing temperature (i.e., less reduction of ΔT in this bending site) than does the molecular structure kinked in the rigid core bearing the hydrogen bond (MS−PA). Moreover, PS−MA (kinked between the core and the flexible part) has the least reduction in ΔT of all systems except the most linear system PS−PA. As a result, various nonlinear shapes affect ΔT values in different ways. Similar to monomer−monomer complexes, ΔT values of monomer−polymer complexes are also in the same order: PS−PPA*m* (the most linear structure) > PS−PMA*m* (kinked between the core and the flexible part) > MS−PPA*m* (kinked in the rigid core bearing the H-bond). On the basis of the modified ΔT data, all PS−MA and PS−PMA*m* systems (kinked between the core and the flexible part) have the second order in ΔT of each series, which suggests that PS−MA and PS−PMA*m* systems with linear H-bonded cores are the most stable complexes (in terms of ΔT) in these kinked supramolecular structures.

N-oxide monomer−monomer complexes do not have the same trend in ΔT values as in the former (non-oxide) comparison. ΔT values of *N*-oxide systems are as follows: PSO−PA (ΔT = −8.1 °C) > MSO−PA (ΔT = −15.4 °C) > PSO−MA (ΔT = −48.6 °C). In addition to XRD results, the clearing temperatures (Table 7) suggest that the schematic structures of *N*-oxide systems may not be as exact as drawn in Figure 6. Hence, the reason for the largest ΔT and large *d* spacing of PSO−PA in *N*-oxide systems is possibly due to the more linear form of the N→O···H−O hydrogen bond in the complexes that is achieved. Nonetheless, ΔT values of *N*-oxide monomer−polymer complexes do not have the same trend as those of monomer−monomer complexes. ΔT values of *N*-oxide monomer−polymer complexes are as follows: PSO−PPA*m* > PSO−PMA*m* > MSO−PPA*m*. Accordingly, the rank increase of ΔT in PSO−PMA*m* reveals that the N→O···H−O hydrogen bond in the monomer−polymer complexes (PSO−PMA*m*) is likely to be more linear than the monomer−monomer

complex (PSO−MA), such that the C−H···O interaction is less effective in the monomer−polymer complexes.

Another interesting result for monomer−monomer complexes is that the *N*-oxide supramolecules show lower clearing (isotropization) temperatures (T_2) and lower ΔT values than their non-oxide analogues, except MSO−PA. For example, PS−PA (ΔT = +41.7 °C) > PSO−PA (ΔT = −8.1 °C) and PS−MA (ΔT = −1.6 °C) > PSO−MA (ΔT = −48.6 °C). Without considering supramolecular shapes, these *N*-oxide systems should have larger T_c (or ΔT) values than their non-oxide analogues by virtue of the stronger dipoles of their constituents. Nevertheless, the molecular structures (e.g., shapes) of these supramolecular complexes cause the reverse effect on the deviation temperatures (ΔT). Consequently, the hydrogen-bonded cores are more highly kinked by insertion of an oxygen atom into their hydrogen bonds (e.g., PSO−PA and PSO−MA), in comparison with their non-oxide analogues (e.g., PS−PA and PS−MA). However, the trend MS−PA (ΔT = −28.9 °C) < MSO−PA (ΔT = −15.4 °C) is opposite to the former results. This can be attributed to a major contribution from their molecular shapes rather than from their dipolar effects. Therefore, both the higher deviation temperatures (ΔT) and higher clearing temperatures (T_2) of MSO−PA may be produced by its more linear structure (Figure 6) compared with that of MS−PA (Figure 5). Overall, structural shape has a more dominant influence on phase behavior than does the dipolar effect in these supramolecular complexes. Concerning monomer−polymer complexes, the supramolecular polymers adopt most of the properties of their monomer−monomer complexes. For instance, the *N*-oxide supramolecular polymers show lower clearing (isotropization) temperatures (T_2) and lower ΔT values than their non-oxide analogues, except MSO−PPA*m*. In addition, PS−PPA*m* > PSO−PPA*m* and PS−PMA*m* > PSO−PMA*m*. As a whole, structural shape also has a remarkable influence on phase behavior in these monomer−polymer complexes.

In general, all these supramolecular polymeric systems have a similar sequence in ΔT values as those of monomer−monomer complexes. Moreover, all monomer−polymer systems have larger ΔT values compared with those of analogous monomer−monomer complexes. This means that positive effects on the clearing temperatures are favored in the kinked supramolecular polymer structures by binding proton donors onto the backbones of the polymers. Thus, these supramolecular polymeric systems have primarily induced more linear structural arrangements than their analogous monomer−monomer complexes. In consequence, the benefit from the shape modification of the hydrogen-bonded cores in the kinked supramolecular polymers does diversify the mesomorphic properties of the hydrogen-bonded structures. There is only one distinct difference in the sequence of ΔT data; i.e., PSO−MA has the last (sixth) rank of ΔT. However, PSO−PMA*m* has the fourth rank of ΔT in each series (m = 3.5, 22, and 35, respectively). For monomer−polymer complexes, the rank of ΔT in PSO−PMA*m* (fourth rank) systems has surpassed those in both MSO−PPA*m* (fifth rank) and MS−PPA*m* (sixth rank) systems, though PSO−MA has a lower (sixth) rank of ΔT than MSO−PA (fourth rank) and MS−PA (fifth rank) in monomer−monomer complexes. This enhancement of ΔT values in PSO−PMA*m* systems suggests that the N→O···H−O hydrogen bond in the monomer−polymer complexes is subject to preserve a more linear core than that of the monomer−monomer complex (e.g., PSO−MA). Consequently, the C−H···O interaction is less sufficient in these kinked PSO−PMA*m* supramolecular polymers. Significantly, the higher molecular weight of PMA*m* causes the higher positive effect on the ΔT value, i.e., ΔT of PSO−MA = −48.6 °C, ΔT of PSO−PMA3.5 = −0.6 °C, ΔT of PSO−PMA22 = +4.5 °C, and ΔT of PSO−PMA35 = +10.1 °C. Hence, it reveals that the less kinked PSO−PMA*m* supramolecular structure has occurred in the higher molecular weight of PMA*m*. For the MSO−PPA*m* supramolecular polymers, because the major binding interaction (O···H−O) will be greatly affected, a large deviation from the ideal geometry in the position of the *N*-oxide is as unlikely to take place in MSO−PPA*m* as that in MSO−PA. Thus, the rank of ΔT in the MSO−PPA*m* supramolecular polymers has not been enhanced in contrast to PSO−PMA*m*. The rank of ΔT in the MS−PPA*m* supramolecular polymers does not improve, either, since the *N*-oxide supramolecule has a more flexible H-bond that can be easily adjusted through binding proton donors onto the backbones of the polymers. Thereafter, because of the higher flexibility of the *N*-oxide H-bond, the kinks in *N*-oxide supramolecular structures are more easily compensated in the monomer−polymer complexes than the kinks in the non-oxide supramolecular structures.

Above all, the *N*-oxide proton acceptors supply us not only with an extra choice of different polarities to induce stronger H-bonding, but also with possible combinations for various shapes of supramolecules. The formation of kinked hydrogen-bonded structures along with the confinement of proton donors onto the backbones of polymers is efficiently applied to improve or to diversify the mesomorphic properties of these supramolecualr side-chain polymers.

Conclusions

In conclusion, novel supramolecular side-chain polymers have formed by connecting the monomers to the proton donor polymers noncovalently. Due to the kinked effects, we are able to tune the shape of the molecular architecture and thus to modify the mesogenic properties and the molecular packings of the supramolecular polymers. Mesogenic properties of the supramolecular side-chain polymers have trends similar to those of supramolecular monomers. However, distinct behavior indeed exists in the supramolecular polymers where the proton donors (acids) are bound to the backbone of the polymer, so the mesomorphic S_A phase is favored and stabilized in the supramolecular polymer structures bearing kinked pendant groups. Compared with their analogous supramolecular monomers (monomer−monomer complexes), higher transition temperatures and wider mesomorphic phases have been observed in all corresponding supramolecular polymers (monomer−polymer complexes). Above all, we have successfully introduced unconventional mesomorphism by bending supramolecules and supramolecular polymers at different positions. Overall, these different shaped isomeric supramolecular polymers with various bending sites and mesomorphic properties supply us with a new way of designing useful liquid crystalline polymers.

Acknowledgment. We would like to thank the Institute of Chemistry, Academia Sinica, and the Na-

tional Science Council of the Republic of China through Grant No. NSC 86-2113-M-001-003 for the financial support of this project.

References and Notes

(1) Lehn, J. M. *Angew. Chem., Int. Ed. Engl.* **1988**, *27*, 89.
(2) Lehn, J. M. *Angew. Chem., Int. Ed. Engl.* **1990**, *29*, 1304.
(3) Stupp, S. I.; Son, S.; Lin, H.-C.; Li, L.-S. *Science* **1993**, *259*, 59.
(4) Stupp, S. I.; Son, S.; Li, L.-S.; Lin, H.-C.; Keser, M. *J. Am. Chem. Soc.* **1995**, *117*, 5212.
(5) Ikkala, O.; Ruokolainen, J.; ten Brinke, G.; Torkkeli, M.; Serimaa, R. *Macromolecules* **1995**, *28*, 7088.
(6) Ruokolainen, J.; Tanner, J.; ten Brinke, G.; Ikkala, O.; Torkkeli, M.; Serimaa, R. *Macromolecules* **1995**, *28*, 7779.
(7) Kotera, M.; Lehn, J. M.; Vigneron, J. P. *J. Chem. Soc., Chem. Commun.* **1994**, 197.
(8) Sato, A.; Kato, T.; Uryu, T. *J. Polym. Sci., Polym. Chem.* **1996**, *34*, 503.
(9) Bazuin, C. G.; Tork, A. *Macromolecules* **1995**, *28*, 8877.
(10) Kumar, U.; Kato, T.; Frechét, J. M. J. *J. Am. Chem. Soc.* **1992**, *114*, 6630.
(11) Kumar, U.; Kato, T.; Frechét, J. M. J. *Adv. Mater.* **1992**, *4*, 665.
(12) Kumar, U.; Frechét, J. M. J.; Kato, T.; Ujiie, S.; Timura, K. *Angew. Chem., Int. Ed. Engl.* **1992**, *31*, 1531.
(13) Kihara, H.; Kato, T.; Uryu, T.; Frechét, J. M. J. *Chem. Mater.* **1996**, *8*, 961.
(14) Kato, T.; Kihara, H.; Ujiie, S.; Uryu, T.; Frechét, J. M. J. *Macromolecules* **1996**, *29*, 8734.
(15) Malik, S.; Dhal, P. K.; Mashelkar, R. A. *Macromolecules* **1995**, *28*, 2159.
(16) Ruokolainen, J.; ten Brinke, G.; Ikkala, O.; Torkkeli, M.; Serimaa, R. *Macromolecules* **1996**, *29*, 3409.
(17) Bazuin, C. G.; Brandys, F. A. *Chem. Mater.* **1992**, *4*, 970.
(18) Brandys, F. A.; Bazuin, C. G. *Chem. Mater.* **1996**, *8*, 83.
(19) Stewart, D.; Imrie, C. T. *J. Mater. Chem.* **1995**, *5*, 223.
(20) Alder, K. I.; Stewart, D.; Imrie, C. T. *J. Mater. Chem.* **1995**, *5*, 2225.
(21) Stewart, D.; Imrie, C. T. *Liq. Cryst.* **1996**, *20*, 619.
(22) Stewart, D.; Imrie, C. T. *Macromolecules* **1997**, *30*, 877.
(23) Lee, J. Y.; Painter, P. C.; Coleman, M. M. *Macromolecules* **1988**, *21*, 954.
(24) Cesteros, L. C.; Meaurio, E.; Katime, I. *Macromolecules* **1993**, *26*, 2323.
(25) Cesteros, L. C.; Isasi, J. R.; Katime, I. *Macromolecules* **1993**, *26*, 7256.
(26) Cesteros, L. C.; Velada, J. L.; Katime, I. *Polymer* **1995**, *36*, 3183.
(27) Kumar, A.; Ramakrishnan, S. *Macromolecules* **1996**, *29*, 8551.
(28) Kumar, A.; Ramakrishnan, S. *Macromolecules* **1996**, *29*, 2524.
(29) Jin, J.-I.; Kang, C.-S.; Lee, I.-H.; Yun, Y.-K. *Macromolecules* **1994**, *27*, 2664.
(30) Willis, K.; Price, D. J.; Adams, H.; Ungar, G.; Bruce, D. W. *J. Mater. Chem.* **1995**, *5*, 2195.
(31) Kato, T.; Adachi, H.; Fujishima, A.; Frechet, J. M. J. *Chem. Lett.* **1992**, 265.
(32) Willis, K.; Luckhurst, J. E.; Price, D. J.; Frechét, J. M. J.; Kihara, H.; Kato, T.; Ungar, G.; Bruce, D. W. *Liq. Cryst.* **1996**, *21*, 585.
(33) Lin, H.-C.; Lin, Y.-S. *Liq. Cryst.* **1998**, *24*, 315.
(34) Lin, H.-C.; Shiaw, J.-M.; Liu, R.-C.; Tsai, C.; Tso, H.-H. *Liq. Cryst.* **1998**, *25*, 277.
(35) Bruce, D. W.; Dunmur, D. A.; Lalinde, E.; Maitlis, P. M.; Styring, P. *Liq. Cryst.* **1988**, *3*, 385.
(36) Lin, H.-C.; Lai, L.-L.; Lin, Y.-S.; Tsai, C.; Chen, R.-C. *Mol. Cryst. Liq. Cryst.*, in press.
(37) Calculations are performed with the Gaussian 94 program: Frisch, M. J.; Trucks, G. W.; Schlegel, H. B.; Gill, P. M. W.; Johnson, B. G.; Robb, M. A.; Cheeseman, J. R.; Keith, T. A.; Petersson, G. A.; Montgomery, J. A.; Raghavachari, K.; Al-Laham, M. A.; Zakrzewski, V. G.; Ortiz, J. V.; Foresman, J. B.; Cioslowski, J.; Stefanov, B. B.; Nanayakkara, A.; Challacombe, M.; Peng, C. Y.; Ayala, P. Y.; Chen, W.; Wong, M. W.; Andres, J. L.; Replogle, E. S.; Gomperts, R.; Martin, R. L.; Fox, D. J.; Binkley, J. S.; Defrees, D. J.; Baker, J.; Stewart, J. P.; Head-Gordon, M.; Gonzalez, C.; Pople, J. A.; Gaussian, Inc., Pittsburgh, PA, 1995. The reported binding energies are results with counterpoise corrections (Boys, S. F.; Bernardi, F. *Mol. Phys.* **1970**, *19*, 553.) for the basis set superposition errors.
(38) For reviews of C−H···O hydrogen bonds: (a) Sarma, J. A. R. P.; Desiraju, G. R. *Acc. Chem. Res.* **1986**, *19*, 222. (b) Desiraju, G. R. *Acc. Chem. Res.* **1991**, *24*, 290. (c) Desiraju, G. R. *Acc. Chem. Res.* **1996**, *29*, 441. (d) Desiraju, G. R. *Angew. Chem., Int. Ed. Engl.* **1995**, *34*, 2311.
(39) If the molecular plane of formic acid is perpendicular to that of pyridine, so that only the N···HO hydrogen bond is possible, the binding interaction reduces from −8.9 to −7.1 kcal/mol.
(40) Iglesias, R.; Serrano, J. L.; Sierra, T. *Liq. Cryst.* **1997**, *22*, 37.
(41) Cai, R.; Samulski, E. T. *Liq. Cryst.* **1991**, *9*, 617.
(42) Watanabe, J.; Hayashi, M. *Macromolecules* **1988**, *21*, 279.
(43) Watanabe, J.; Hayashi, M. *Macromolecules* **1989**, *22*, 4083.
(44) Coates, D. In *Liquid Crystals − Application and Uses*; Bahadur, B., Ed.; World Scientific: Singapore, 1990; Vol. 1, Chapter 3.

MA980720E